

Application of the  
Computational Fluid Dynamics Solver FLUENT  
to  
Keels of Sailing Yachts

*Master Thesis*  
J.H.S. de Baar  
TU Delft  
June 18, 2010

*Committee*  
prof. dr ir R.H.M. Huijsmans  
dr ir J.A. Keuning  
dr ir M.J.B.M. Pourquoi  
dr ir M.I. Gerritsma



## **Abstract**

The keel of a sailing yacht has been shown to constitute a significant part of the overall resistance. Where the details of this effect are not yet fully understood, Computational Fluid Dynamics (CFD) analysis might reveal mechanisms unseen to the experimental eye.

An important step in CFD application is the simulation of a number of validation cases. In the present study I simulate three different validation cases in the commercial CFD solver FLUENT, applying a Reynold's Averaged Navier-Stokes (RANS) method with a realizable  $k - \epsilon$  turbulence model and a Volume of Fluid (VOF) free-surface approach. From these three validation cases I obtain five drag coefficients, four of which are within an acceptable range of error of the experimental values.

After this validation, I consider several mechanisms related to keel resistance. Simulations indicate that the keel rudder interaction is Froude scaled and that the keel resistance can be scaled by a form factor method, presumably by means of a flat plate skin friction line.

### Idee 156

Een boekhouder, een rekenaar, kan zich vergissen. De Noodzakelykheid nooit. Ander voorbeeld. Gegeven 'n schip met zóóveel diepgang, zóóveel tegenstand, zóóveel zeilen, enz. De wind blaast op die zeilen met gegeven kracht, en uit 'n gegeven hoek. Stel alle noodige opgaven bekend, dat ze niet kunnen wezen omdat er zooveel factoren aan ons gebrekkig waarnemingsvermogen ontsnappen. Wordt gevraagd: de snelheid van 't vaartuig? Die berekening is niet gemakkelyk, en wat volkomen juistheid aangaat onmogelyk. De Noodzakelykheid weet het. Haar ontsnapt niets. Zy brengt alles in rekening, tot de wryving van 't vischje dat zich schuurde tegen 't scheepsboord, tot den invloed van den wind op 'n hoofdhaar van den schepeling, tot den tegenstand van 'n zwevend schuimbolletje voor den boeg, tot de verplaatsing van 'n atoom gas in de lading... alles! Zy weet de snelheid waarmee 't schip zich moet bewegen volgens de háár alleen bekende gegevens, en ze noemt die snelheid, drukt ze uit: door het feit!<sup>1</sup>

Multatuli, 1862

### Idea 156

An accountant, a clerk, can make mistakes. Necessity never. Other example. Take a ship with a certain draw, a certain resistance, so many sails etc. The wind blows on those sails with a given force and from a given angle. Assume all necessary components are known, which they can not possibly be because so many factors escape our limited powers of observation. Asked: speed of the vehicle? That calculation is not easy and concerning correctness impossible. Necessity knows it. Nothing escapes her. She accounts for everything down to the friction of the little fish which rubbed against the hull of the ship, down to the influence of the wind on the hair of the sailor, down to the resistance of a floating bubble of foam in front of the bow, down to the displacement of single atom of gas in the cargo. . . Everything! She knows the speed at which the ship has to propel itself, according to the factors known only to her, and she names this speed, expresses it: through the fact!<sup>1</sup>

Multatuli, 1862

---

<sup>1</sup>Multatuli, *Ideeen*, I.G.L. Funke, Amsterdam (1897), translation by Claire Evans



# Contents

<b>1</b>	<b>Introduction</b>	<b>7</b>
<b>2</b>	<b>Method</b>	<b>9</b>
2.1	Dimensional Analysis . . . . .	9
2.2	Experimental Setup . . . . .	10
2.3	Mathematical Model . . . . .	11
2.3.1	Governing Equations . . . . .	11
2.3.2	Discretization . . . . .	11
2.3.3	Turbulence Model . . . . .	12
2.3.4	Wall Treatment . . . . .	12
2.3.5	VOF Method . . . . .	12
2.3.6	Existence of a Solution . . . . .	13
2.3.7	Symmetry and Vortex Shedding . . . . .	13
2.4	Grid . . . . .	13
2.4.1	Grid Generation . . . . .	14
2.4.2	Grid Convergence and Error Estimation . . . . .	14
2.5	Summary of Simplifications . . . . .	15
<b>3</b>	<b>Benchmark Problems</b>	<b>17</b>
3.1	Sphere Drag . . . . .	17
3.2	NACA 63-010 Section Drag . . . . .	19
3.3	NACA 63-010F Section Drag . . . . .	20
3.4	Broken Dam . . . . .	21
3.5	Surface Piercing Hydrofoil . . . . .	22
3.6	Conclusions . . . . .	24
<b>4</b>	<b>2-Dimensional Grid and Boundary Choices</b>	<b>25</b>
4.1	Asymptotic Range . . . . .	25
4.2	Turbulence Stimulation Strips . . . . .	25
4.3	Rudder Effect . . . . .	28
4.4	Surface Roughness . . . . .	28
4.5	Conclusions . . . . .	29
<b>5</b>	<b>Validation for the Bare Hull</b>	<b>31</b>
5.1	Grid . . . . .	31
5.2	Wall $y^+$ . . . . .	31
5.3	Time Convergence . . . . .	31
5.4	Grid Convergence, Richardson Extrapolation . . . . .	32
5.5	Conclusions . . . . .	32
<b>6</b>	<b>Validation for the Keel Hull Combination</b>	<b>35</b>
6.1	Grid . . . . .	35
6.2	Wall $y^+$ . . . . .	36
6.3	Time Convergence . . . . .	36
6.4	Grid Convergence, Richardson Extrapolation . . . . .	37
6.5	Wave Height . . . . .	38

6.6	Conclusions . . . . .	38
<b>7</b>	<b>Practical Implications</b>	<b>41</b>
7.1	Keel Rudder Interaction . . . . .	41
7.2	Scaling Keel Rudder Interaction . . . . .	44
7.3	Scaling Keel Drag . . . . .	46
7.4	Conclusions . . . . .	46
<b>8</b>	<b>Discussion</b>	<b>51</b>
8.1	Strengths . . . . .	51
8.2	Weaknesses . . . . .	51
8.3	Opportunities . . . . .	52
8.4	Threats . . . . .	52
	<b>Acknowledgments</b>	<b>53</b>
	<b>References</b>	<b>55</b>
	<b>List of Figures</b>	<b>56</b>
	<b>List of Tables</b>	<b>58</b>
<b>A</b>	<b>Symbols and Acronyms</b>	<b>59</b>
<b>B</b>	<b>Details for Chapter 7</b>	<b>60</b>
<b>C</b>	<b>FLUENT Settings</b>	<b>61</b>
C.1	Benchmark Problems . . . . .	61
C.2	Validation for the Bare Hull . . . . .	62
C.3	Validation for the Keel Hull Combination . . . . .	63
<b>D</b>	<b>What did not work ...</b>	<b>64</b>
D.1	Benchmark Problems . . . . .	64
D.2	Validation for the Bare Hull . . . . .	64
D.3	Validation for the Keel Hull Combination . . . . .	64
D.4	General Suggestions . . . . .	65





*Australia II* leading *Liberty* in the 1983 America's Cup. *Australia II*'s innovative keel has been a landmark for the application of Computational Fluid Dynamics in sailing yacht design. ©Barbara Y.E. Pyle, from Ref [1]

# Chapter 1

## Introduction

Computational Fluid Dynamics (CFD) has been applied to various sports, including Formula 1 racing, rowing, swimming, and sailing [2, 3, 4]. CFD aims to provide reliable estimates of physical quantities, while at the same time it aspires to improve understanding of the mechanisms involved. Ultimately, this knowledge can invoke innovations that give the athlete an edge in the competitive arena.

Despite its numerous successes, CFD can easily lead to confusing or inadequate results. It is our task to test CFD for any new application. Such a test, or validation case, encompasses the CFD simulation of a complete physical experiment. The ability to reproduce the results that were observed in the experiment is the trial that CFD stands.

For various types of ships there have been several promising validation cases, including those for sailing yachts [5, 6, 7]. However, none of these cases have explicitly addressed the resistance of the keel of the sailing yacht. The TU Delft has extensive experimental data on the resistance of various keel hull combinations [8, 9, 10]. These data facilitate a validation case that distinguishes between the hull resistance and the keel resistance.

The hypothesis for the present study is: A simulation with the commercial CFD solver FLUENT provides adequate estimates for both the hull resistance and the keel resistance of a sailing yacht.

The simulations indicate that in most cases this hypothesis is correct. Regarding the understanding of mechanisms, the simulations suggest that the keel rudder interaction is Froude scaled, that the keel resistance can be scaled by means of a form factor method, and that the keel resistance might best be scaled by a flat plate skin friction line.

The present study continues previous studies by the novel combination of: specific keel resistance, structured grids, grid convergence studies, and simulation error estimates.

First I explain the experimental setup and mathematical model in Chapter 2, apply it to some simple problems in Chapter 3, and analyze some 2-dimensional cases in Chapter 4 in order to simplify the simulations. In the main part of the report I validate the simulations for the bare hull in Chapter 5, and for two keel hull combinations in Chapter 6. After the validation I discuss several practical implications in Chapter 7. The report is then completed by a discussion.



The Zen garden at Ryoanji Temple (Kyoto, Japan). Like a mathematical model, the garden itself is quite sterile. It will only reveal it's true beauty upon carefull observation and - eventually - interpretation. ©Jouke de Baar

# Chapter 2

## Method

In the present study, the experiment and the simulation are in close relation. On the one hand the numerical model - which in itself might be very interesting - remains useless without proper validation; without the ability to reproduce the experimental results. On the other hand, the experiments leave questions unexplained; questions to be answered by physical information that is obviously there but remains unseen to the experimental eye. Such questions might well be resolved by analysis and interpretation of the calculated results. To fully understand this relation, it is important to have some knowledge of both the experimental setup and the numerical model.

In this chapter, it is my objective to focus on the choices made, to explain why I consider certain models appropriate. In order to maintain this focus I have decided to limit the amount of equations and refer to the literature instead.

### 2.1 Dimensional Analysis

The aim of this section is to present the experimental and computational data in dimensionless form. Such a presentation simplifies the data and thus helps to understand the results. The correct dimensionless parameters are found by means of a dimensional analysis, as presented by Ipsen [11].

Assume that the drag force  $F$  on a certain object moving through a fluid is determined by the following parameters: a characteristic object size  $L$ , the velocity  $u_\infty$ , the fluid density  $\rho$ , the fluid viscosity  $\mu$ , and the gravitational acceleration  $g$ . Ipsen's method then results in two dimensionless quantities, the Reynold's number:

$$Re = \frac{\rho u_\infty L}{\mu} \quad (2.1)$$

and the Froude number:

$$Fn = \frac{u_\infty}{\sqrt{gL}} \quad (2.2)$$

Together, these two quantities characterize the complete flow. In large part, the viscous effects are characterized by the Reynold's number whereas the free-surface effects are characterized by the Froude number. The drag coefficient:

$$C_D = \frac{F}{\frac{1}{2}\rho u_\infty^2 S} \quad (2.3)$$

then acts as the dimensionless drag force, where  $S$  is the wetted surface. For this specific object, we now assume that the drag coefficient depends exclusively on the Reynold's number and the Froude number. Unless specified differently, in this study the Froude number is based on the waterline length of the hull, while the Reynold's number is based on the mean chord length of the keel.

## 2.2 Experimental Setup

Ship model testing involves an array of difficulties known as the scaling problem [12]. Because these simulations are at the same model scale as the experiments, most scaling issues will not arise. However, one important aspect of the scaling problem is that in the International Towing Tank Committee (ITTC) method the model is at the same Froude number but at a lower Reynold's number than the actual ship [13]. This would result in a lack of turbulence in the model setup. As a remedy, the model is equipped with turbulence stimulation strips, the effect of which I will study in Chapter 4.

The hull used in the experiments [9] is TU Delft hull number 366, the lines are shown in Figure 2.1. It is a lower beam/draft ratio version of hull number 329, which is a typical International America's Cup Class (IACC) hull scaled by a factor 1:7. Underneath the hull is - turn by turn - one of the keels shown in Figure 2.2. The main dimensions of the hull, keels, and rudder (which will not be present in the simulation) are tabulated in Tables 2.1 and 2.2. The keel profiles do not have the sharp NACA 63 trailing edge, but have a 2 mm wide flattened edge.

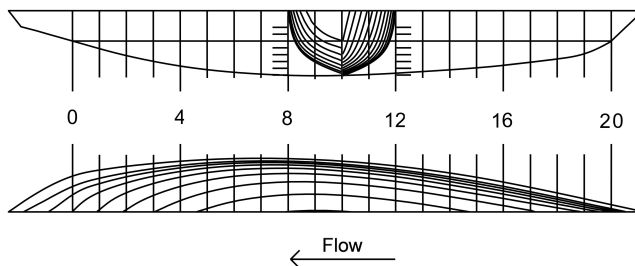


Figure 2.1: The 366 hull as used in the simulations. The top view displays the sections of the hull, together with a side contour. The bottom view displays the waterlines. Geometry from Ref. [9, 10]

Table 2.1: Hull Dimensions [8]

Length on Waterline	2.74	$m$
Beam on Waterline	0.487	$m$
Draft	0.159	$m^2$
Displacement	0.071	$m^3$
Wetted Surface	1.114	$m^2$

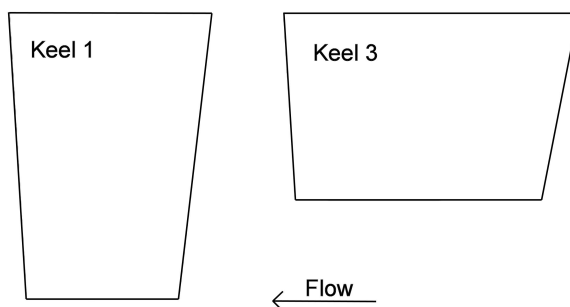


Figure 2.2: The planforms of the different keels. From Ref. [9]

The Delft Ship Hydromechanics Laboratory towing tank is 145 m long, 4.5 m wide and 2.5 m deep. During the tests the model is attached rigidly in all six degrees of freedom (surge, sway, heave, roll, pitch, and yaw). The model is towed at different speeds, ranging from a Froude number of 0.10 to 0.60. The model has turbulence stimulation by means of carborundum strips on the hull, keel, and rudder. In this experiment, strips of 2.0 cm wide are placed on the hull at 0 cm, 76 cm, and 133 cm from the



Table 2.2: *Appendage Dimensions [9]*

	Keel 1	Keel 3	Rudder	
Span	0.374	0.245	0.321	<i>m</i>
Mean Chord	0.231	0.352	0.115	<i>m</i>
Wetted Surface	0.176	0.177		<i>m</i> <sup>2</sup>
Profile	NACA-63	NACA-63		-
Thickness/Chord	0.10	0.066	0.14	-

bow waterline. A strip of 1.5 cm wide is placed at 1.5 cm from the leading edge of the keel. Finally, a strip of 1.0 cm wide is placed at 1 cm from the leading edge of the rudder.

The total drag is measured, as well as the drag experienced directly by both the keel and the rudder. For the validation I consider the zero heel, zero leeway drag coefficients for a Froude number of 0.35, that is a model velocity of  $u = 1.80$  m/s. The experiments indicate that for low Froude numbers viscous effects are dominant, while for high Froude numbers free-surface effects are more important. At this intermediate Froude number of 0.35 both the viscous and free-surface effects can be expected to play an important role, which makes it interesting for validation.

## 2.3 Mathematical Model

The mathematical model involves the choice of a reference system. The origin is located on a fixed position close to the center of the hull, on the waterline directly above the level hull center of displacement. The  $x$ -direction is along the incoming flow direction (towards the stern of the hull), the  $y$ -direction points horizontally to starboard, and the  $z$ -direction points vertically upwards.

### 2.3.1 Governing Equations

Assume that a fluid in the domain  $\Omega$  is described completely by<sup>1</sup> the density  $\rho$ , the velocity  $\vec{u}$ , the pressure  $\tilde{p}$ , and the viscosity  $\mu$ . The governing equations for conservation of mass and momentum are [11, 14, 15]:

$$\begin{aligned} \partial_t \rho + \nabla \cdot (\rho \vec{u}) &= 0 \\ \partial_t(\rho \vec{u}) + \nabla \cdot (\rho \vec{u} \otimes \vec{u}) &= -\nabla \tilde{p} + \nabla \cdot \hat{\tau} + \rho \vec{g} \end{aligned} \quad (2.4)$$

For a Newtonian fluid the stress tensor  $\hat{\tau}$  is:

$$\hat{\tau} = \mu \left[ (\nabla \vec{u} + \nabla \vec{u}^T) - \frac{2}{3} \nabla \cdot \vec{u} I \right] \quad (2.5)$$

where  $\mu$  is the dynamic viscosity and  $I$  is the unit tensor.

These governing equations are the Navier-Stokes Equations.<sup>2</sup> Since water is highly incompressible, the problem is treated as an incompressible flow. Applying a time average filter results in the Reynold's Averaged Navier-Stokes (RANS) equations, which effectively have an additional term in the momentum equation known as the Reynold's stress tensor. The Reynold's stress tensor can be calculated from a turbulence model. Since the complete flow will be considered to be in the turbulent regime (due to the turbulence stimulation strips), application of the reduced Euler Equations is not appropriate.

### 2.3.2 Discretization

In order to analyze the flow numerically, the physical domain is first discretized into grid cells. The flow variables are subsequently assigned to each of the cells. It is therefore necessary to discretize the

<sup>1</sup>The pressure  $\tilde{p}$  has a wiggle, to discriminate it from the convergence order  $p$ .

<sup>2</sup>The complete Navier Stokes Equations also include conservation of energy. I choose to drop this third equation because it is of no importance in an incompressible flow without significant thermal effects. I performed a validation case with and without the Energy equation and, indeed, the effect was minimal.

governing equations. This model applies a Finite Volume Method with a  $2^{nd}$  order upwind discretization scheme [16]. Compared to the  $1^{st}$  order upwind scheme, the  $2^{nd}$  order upwind scheme provides a higher grid convergence order and better accuracy of the discretization.

### 2.3.3 Turbulence Model

The flow will exhibit turbulence on different scales. In order to explicitly model all relevant turbulence scales, the number of cells in the discretized domain should be in the order  $Re^{\frac{9}{4}}$  [17]. The present problem has a Reynold's number in the order of  $Re = 1 \times 10^6$ , which would require over  $10^{13}$  cells in the domain. This would require a  $10^7$  GB RAM machine, which is considerably larger than the typical 10-20 GB RAM machines available for these kind of calculations.

The remedy is to have a much smaller number of cells and model the turbulent effects associated with scales smaller than the scale of the cells with a turbulence model. There are various models available. Since the present model is likely to exhibit separation and recirculation at the flattened trailing edge of the keel, the best option is the Realizable  $k - \epsilon$  Model [14, 15, 18]. This is also the best performing turbulence model in a comparative validation case for a backward facing step [19], where the backward facing step is similar to the flattened trailing edge of the keel. Another benefit of the model is that it limits the unphysical growth of  $k$  at the leading edge stagnation point [20].

The model consists of two transport equations, one for the turbulent kinetic energy  $k$  and one for the turbulent dissipation rate  $\epsilon$ . It contains several empirically determined constants, in the present simulation the values are:  $\sigma_k = 1.0$ ,  $\sigma_\epsilon = 1.2$ ,  $C_2 = 1.9$ , and  $C_{1\epsilon} = 1.44$  [14].

The Reynold's stress tensor can be calculated directly from  $k$  and  $\epsilon$ , such that it can be applied in the RANS momentum equation [14].

### 2.3.4 Wall Treatment

A turbulent flow near a wall can be characterized by the dimensionless velocity  $u+$  and dimensionless wall distance  $y+$ , which are related to the local wall shear stress  $\tau_w$  [14, 15]:

$$u+ = u \sqrt{\frac{\rho}{\tau_w}} \quad , \quad y+ = \frac{\rho y}{\mu} \sqrt{\frac{\tau_w}{\rho}} \quad (2.6)$$

Close the wall,  $u+$  varies rapidly with  $y+$ . To illustrate this dependency I have simulated the boundary layer of a flat plate. The simulation has a very fine grid close to the wall (it is a near wall simulation with wall  $y+=0.02$ ). The velocity profile is shown in Figure 2.3, together with experimental results. The profile has four different layers: the viscous sublayer, the mixing layer, the Logarithmic layer and the outer layer. For the viscous sublayer and the Logarithmic layer it is possible to approximate the results with either a Linear or a Logarithmic Law of the Wall [14, 15]. Both laws are indicated in the figure.

It is impractical to model the complete boundary layer in each simulation, as it would require a very fine grid. Instead, it is possible to have the first cell in either the viscous sublayer or the Logarithmic layer while adjusting the wall boundary condition to comply with the corresponding Wall of the Law. For a proper application the  $y+$  of the first cell center, which is known as wall  $y+$ , should either be wall  $y+ \leq 5$  (viscous sublayer) or  $30 \leq \text{wall } y+ \leq 300$  (Log layer) [14].

In FLUENT the Standard Wall Function is a two layer model which applies either the Linear Law or the Logarithmic Law boundary condition, depending on wall  $y+$ . The Enhanced Wall Treatment is a blended version of the two layer model of a more general application [14].

### 2.3.5 VOF Method

Since this is a stratified free-surface problem on a stationary grid I use the Volume of Fluid (VOF) Method [14, 22]. This method solves the fraction of water in each grid cell. The Geometric Reconstruction scheme assumes that the free-surface has a linear slope in each grid cell. Any other scheme resulted in an overly smudged free-surface.

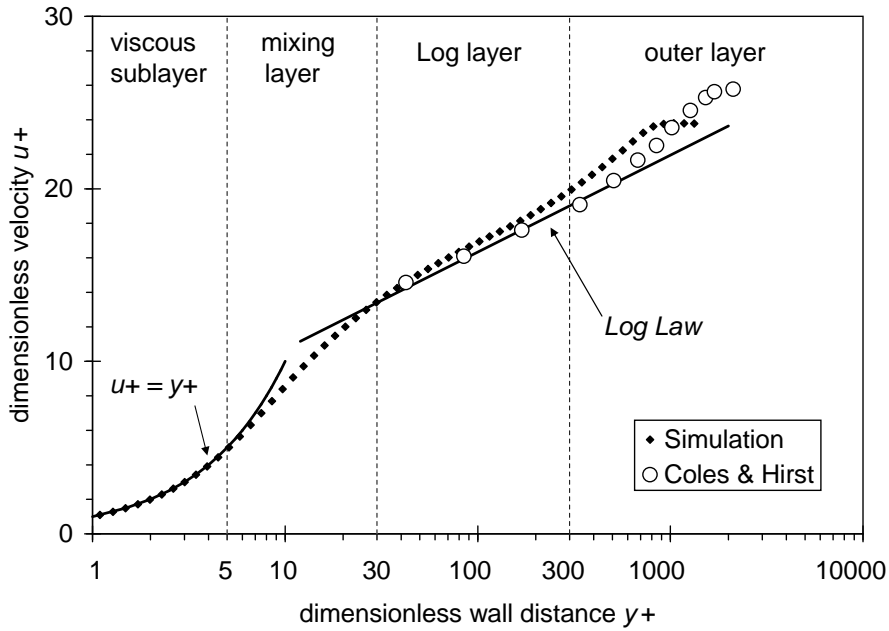


Figure 2.3: Turbulent flat plate boundary layer. The arrows indicate the two Wall Laws, which apply in the viscous sublayer and in the Log layer. The exact starting position of the outer layer depends on the Reynold's number. The Linear and Log Law are from Ref. [14, 15], the simulation is a near-wall simulation (wall  $y^+ = 0.02$ ), and the experimental results by Coles & Hirst are from Ref [21]

### 2.3.6 Existence of a Solution

For the physical experiment it is quite clear that setting it up will lead to some physical result. For the computational model this is not necessarily true. The model set up in the previous sections might very well turn out to have no solution at all. It should be noted that up to this date there is no proof of the existence of a smooth solution of the Navier-Stokes Equations for a general 3-dimensional problem. In fact, finding this proof was declared one of the million dollar problems in mathematics for this millennium [23].

When the Realizable  $k - \epsilon$  Model is included, the proof becomes somewhat easier, although again there is no proof of a solution for a general 3-dimensional problem. For a reduced model however, it can be shown that a solution exists [15].

### 2.3.7 Symmetry and Vortex Shedding

The symmetry of the problem suggests application of a symmetry plane in the  $xz$ -plane of the simulation. However, this is only possible if there are no asymmetric effects. One of the asymmetric effects that might arise from the flattened (or 'blunt') keel trailing edge is vortex shedding. A similar case [24] shows this is likely to occur when the flattened edge based Reynold's number  $Re_{edge} \geq 1.9 \times 10^4$ , whereas in the present simulation it is only  $Re_{edge} = 3.6 \times 10^3$ . Therefore I do not expect vortex shedding and make use of a symmetry plane.

## 2.4 Grid

The division of the computational domain into a discrete number of cells is known as a grid. Some care has to be taken in creating the grid, as poor grid quality will have a negative effect on convergence and on the reliability of the calculated results.

### 2.4.1 Grid Generation

Grids can be either unstructured or structured. Figure 2.4 shows a 2-dimensional example of a grid around a sphere. It can be seen that in the structured case, each grid cell has four distinct neighbors. This will increase the solver speed as it is easier to find the flow variable in neighboring cells, since they are simply the next cell in the numerical storage array.<sup>3</sup> Another benefit of the structured grid is that it is easier to align the cells with the expected streamlines, thus minimizing numerical diffusion. Therefore, I use structured grids in this study.

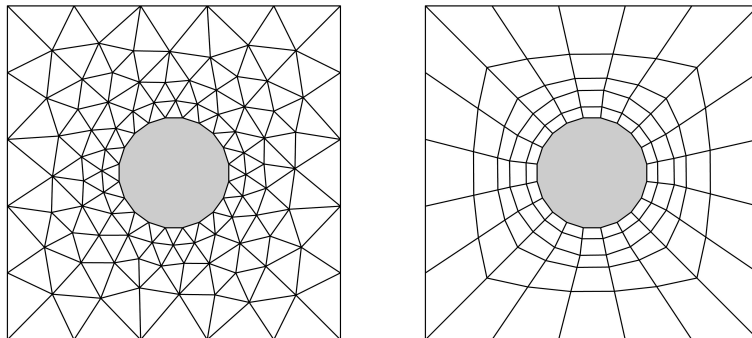


Figure 2.4: *Examples of an unstructured (left) and a structured (right) grid around a 2-dimensional sphere*

A structured grid comes in different typical layouts. As illustrated in the right of Figure 2.4 a sphere invites a circular shaped grid which is known as an O-Grid. The wing like geometry displayed Figure 2.5 invites an asymmetric layout, known as a C-Grid. These are the two grid layouts I will use.

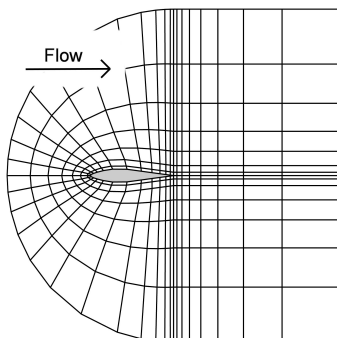


Figure 2.5: *Different geometries invite different grid layouts. On the right of the previous figure is an O-Grid around a 2-dimensional sphere, while this figure displays a C-Grid around a wing section*

An essential part of grid generation is to have the wall adjacent cell either in the viscous sublayer or in the Logarithmic layer. Therefore, all simulation results come with the area averaged wall  $y^+$  of the surfaces involved. Note that there is no exact *a priori* method to determine the first cell width. This means that grids often have to be regenerated with a more appropriate wall cell thickness.

All grids are generated in GAMBIT, which is distributed with the FLUENT package.

### 2.4.2 Grid Convergence and Error Estimation

The discretization results in a simulation error. In general, a finer grid is expected to show a smaller error. It can be assumed that in a certain grid size range, known as the 'asymptotic range', the simulation result  $f_h$  can be expressed as a polynomial in the typical grid cell size  $h$ . Since the method is  $2^{nd}$  order, the  $h^2$  term is likely to dominate this polynomial [25]:

$$f_h = f_0 + g_1 h + g_2 h^2 + O(h^3) \quad (2.7)$$

<sup>3</sup>Although it is not clear whether this is actually being utilized by FLUENT

where  $f_0$  is the exact solution.

If the problem is simulated on three grids of different refinement, it is possible to calculate an observed order of convergence  $p$ , which due to a number of reasons can differ from the  $2^{nd}$  order of the discretization. With knowledge of the observed  $p$ , it is then possible to make a Richardson Extrapolation and calculate a Grid Convergence Index (GCI) [25, 26]. The extrapolation gives a more accurate simulation result, the GCI gives an estimate of the error in that result.

Chapter 4 provides a rough 2-dimensional estimate of the asymptotic range for the keel and hull grids. Then, after simulating the 3-dimensional case, I verify that the grids are indeed in the asymptotic range. This can be done by means of the coarse to medium grid  $GCI_{cm}$ , the medium to fine grid  $GCI_{mf}$ , the refinement factor  $r$  and the observed order of convergence  $p$ . The requirement is that the ratio [25]:

$$\frac{GCI_{cm}}{r^p GCI_{mf}} = 1 \quad (2.8)$$

The GCI involves the choice of a safety factor. It should be 3.0 for studies based on two grids, and 1.25 for studies based on three grids. Only two out of the five 3-dimensional drag coefficients are based on three grid studies, whereas the remaining three drag coefficients are based on two grid studies. Therefore I choose the more conservative 3.0 safety factor.

## 2.5 Summary of Simplifications

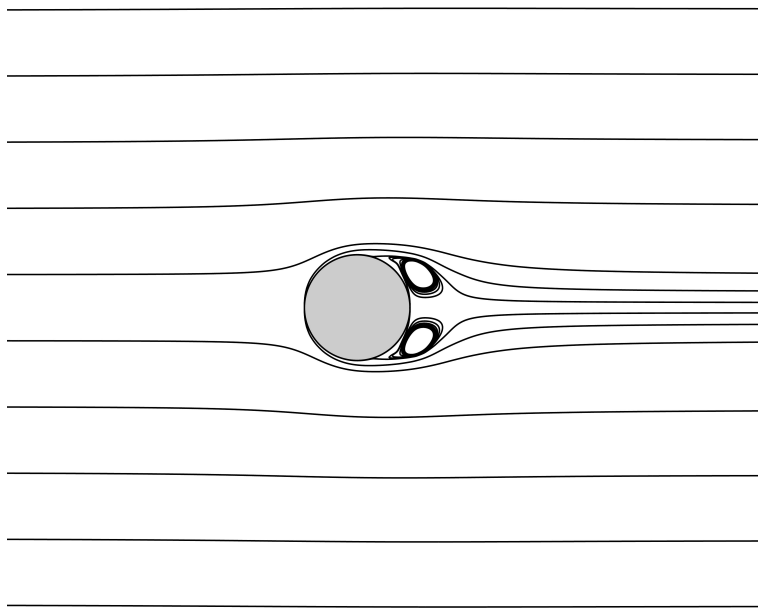
The simulations of the bare hull and the keel hull combinations contain a number of simplifications. Most of these simplifications were addressed in the previous sections, a number of simplifications will be addressed in Chapter 4.

The following simplifications are all ready present in the selected experimental cases:

- All effects at model scale
- Measurements made for constant velocity
- No heel or leeway
- Fixed heave and pitch
- No wind or waves
- (Stimulation of) Fully turbulent flow
- Tank floor and walls limit the domain
- Air drag is neglected
- Hull and keel surface are smooth

The simulation has the following additional simplifications:

- Homogeneous fluid (including incompressibility)
- Newtonian fluid
- Application of the RANS equations
- Discretization
- Application of the Realizable  $k - \epsilon$  Turbulence Model
- Wall Treatment
- Application of the VOF Model
- Assumption of an asymptotic range of simulation error (verified in Chapters 4, 5, and 6)
- Richardson Extrapolation
- Upstream (1 LWL) and downstream (2 LWL) domain limits
- Perfectly smooth tank wall and bottom
- No turbulence stimulation strips (verified in Chapter 4)
- No rudder (verified in Chapter 4)
- Perfectly smooth hull and keel surface (verified in Chapter 4)



Calculated pathlines of the flow around a sphere at a Reynold's number of 1000. The flow around a sphere is an example of a simple problem with well known results, which offers the possibility of a straightforward validation of the computational results.

## Chapter 3

# Benchmark Problems

A first step in the validation of a Computational Fluid Dynamics (CFD) method is the calculation of a number of benchmark problems. These are relatively simple problems in terms of geometry and required CPU time. Also, the available experimental data offers a straightforward validation of the computational results. These benchmark problems serve both as an exercise in CFD modeling and a challenge to the CFD method.

Furthermore, the problems offer an illustration of several issues involved in CFD modeling. I have selected a number of problems which illustrate: the effect of grid size; the effect of the discretization scheme; the effect of physical detail; time evolution; and the free-surface. All issues illustrated here were discussed - in theory - in the previous chapter.

### 3.1 Sphere Drag

A sphere moving through a fluid will experience a drag force. The drag coefficient at different Reynold's numbers is well known from a wide range of experiments. For example, one review article selects 480 data points from over 40 different experiments [27]. An extensive CFD validation for this same problem also refers to a range of experiments [28]. The large number of experimental results has resulted in textbook drag coefficients based on such experiments [29, 30]. These textbook values are the experimental values I will use here. A distinct effect exhibited by the data is a sudden drop of the drag coefficient - the 'drag crisis' - near  $Re = 3 \times 10^5$ .

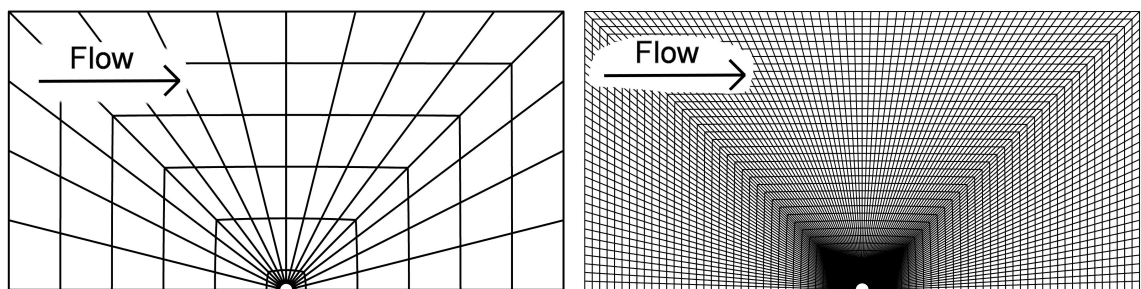


Figure 3.1: *Different grids used for calculation of the sphere drag coefficient. The bottom of the grid is the axis of rotation. The finer grid is likely to give more accurate results*

Since the problem is axisymmetric, the mesh is 2-dimensional. The mesh is shown in Figure 3.1. The size of the mesh is 8192 cells. The width of the cells at the sphere boundary is 0.15 mm, resulting in a wall  $y_+ = 1.7 \pm 0.8$  at<sup>1</sup> the 'drag crisis' point  $Re = 3 \times 10^5$ . This permits the application of Enhanced Wall Treatment. Detailed FLUENT settings are listed in the Appendix for all problems.

---

<sup>1</sup>All wall  $y_+$  are calculated for wall adjacent cell center.

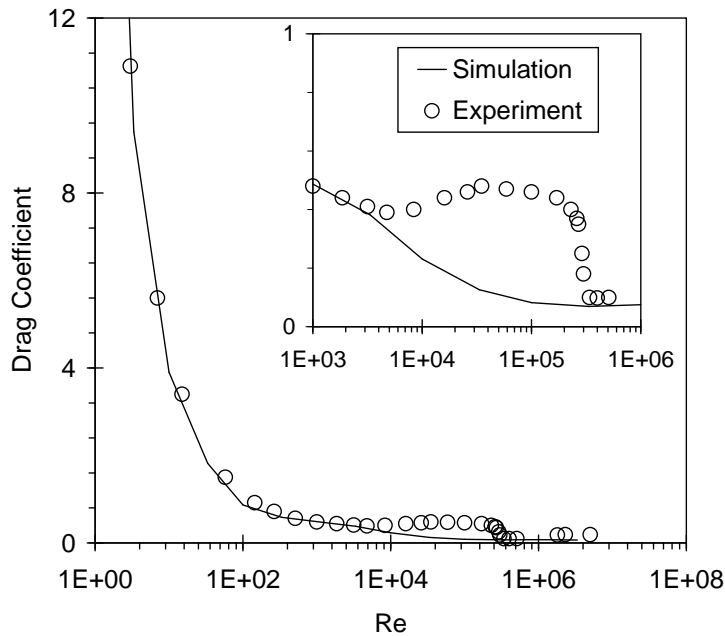


Figure 3.2: Sphere drag coefficient at different Reynold's numbers. The insert is a detail of the  $Re = 10^3$  to  $Re = 10^6$  region, displaying the absence of a distinct 'drag crisis' in the calculated results. Experimental values from Ref. [29]

The calculated drag coefficients are shown in Figure 3.2. The turbulence model was active over the whole range of Reynold's numbers, although at lower Reynold's numbers the effect is minimal. For example, at  $Re = 10$  the turbulent viscosity ratio is less than  $10^{-19}$ . As can be seen, the results agree well with the experimental values, except for the region of a Reynold's number of roughly  $5 \times 10^3 - 2 \times 10^5$ . In this region the calculated results do not show a distinct 'drag crisis'. One could state that the model is unable to capture the transition from the (low Reynold's number) laminar regime to the (high Reynold's number) turbulent regime. The absence of a 'drag crisis' is an obvious shortcoming of this simple axisymmetric model.

The sphere drag problem serves well to illustrate the effect of the grid size. A larger number of cells is expected to reduce the error in the solution, where the error is given by the difference between the computational and the experimental drag coefficient. This trend is illustrated by Figure 3.3. It can be expected that such a figure shows a linear upper bound on the error, and that the slope of this upper bound is equal to the discretization order - which in this case is two. These expectations agree well with the linear regression shown in Figure 3.3, which has a correlation coefficient of 0.96 and a slope of 1.84.



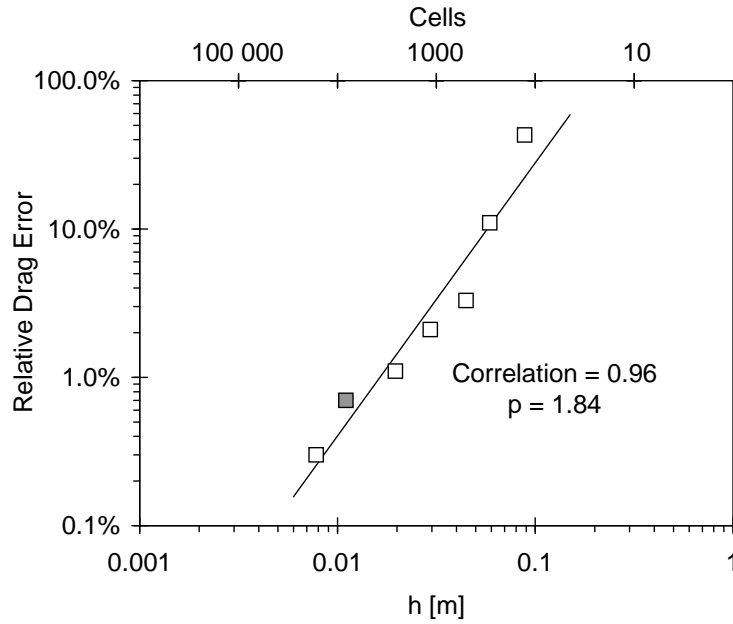


Figure 3.3: The effect of the grid size on the solution error at  $Re=1000$ . The gray faced label indicates the grid used in the above calculations

### 3.2 NACA 63-010 Section Drag

The National Advisory Committee for Aeronautics (NACA) has designed a number of wing sections. The NACA 63-010 wing section is the basis for the Delft Systematic Keel Series (DSKS). Initially I intended to compare the results to the data provided for the NACA 63 series [31]. However, since in the experiments the flow is partially laminar, this approach proved inadequate. Therefore I compare the results to the fully turbulent flat plate skin friction line<sup>2</sup> by Anderson [32, 33]:

$$C_F^{And} = \frac{0.074}{Re^{1/5}} \quad (3.1)$$

Since a wing section is a cut of an infinitely long wing, the model is 2-dimensional. The grid contains 8640 cells, a detail of the grid is shown in Figure 3.4. The grid uses symmetry, such that only the upper half of the problem is modeled. The width of the cells at the NACA section boundary is 0.03 mm, resulting in a wall  $y^+ = 3.4 \pm 1.0$  at  $Re = 1 \times 10^6$ . For higher Reynold's numbers the cell width at the boundary was reduced to 0.003 mm, resulting in a wall  $y^+ = 2.6 \pm 0.6$  at  $Re = 1 \times 10^7$ . This permits the application of Enhanced Wall Treatment.



Figure 3.4: Detail of the NACA 63-010 grid

The calculated drag coefficients are shown in Figure 3.5. The results illustrate the dramatic effect of changing the discretization scheme from 1<sup>st</sup> order upwind to 2<sup>nd</sup> order upwind: the corresponding drag coefficients are reduced by roughly a half.

<sup>2</sup>This is the total skin friction coefficient  $C_F$ , different from the local skin friction coefficient  $c_f$

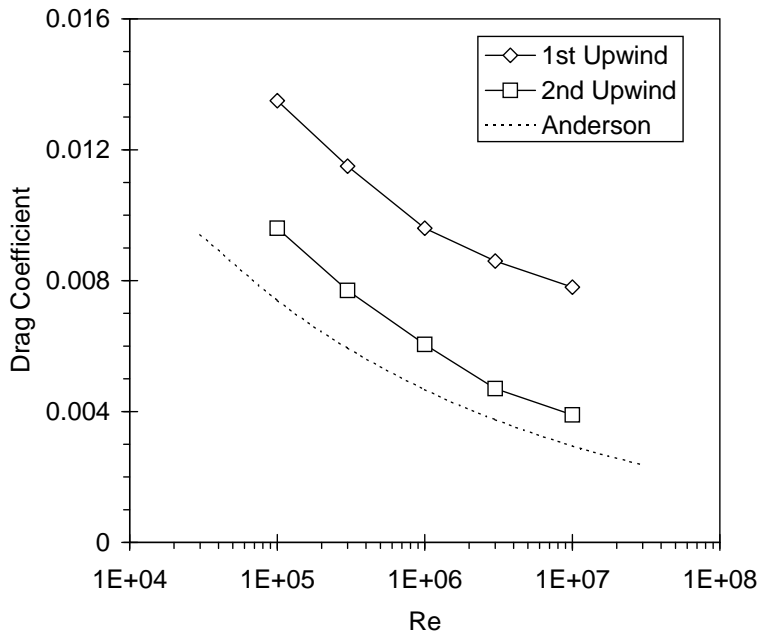


Figure 3.5: NACA 63-010 drag coefficient. The Anderson fully turbulent flat plate skin friction line is from Ref. [32]

### 3.3 NACA 63-010F Section Drag

The NACA 63-010 section of the previous problem has an infinitely sharp trailing edge. In reality, the DSKS keels have a 2 mm wide flattened trailing edge. The flattened trailing edge section is modeled by the NACA 63-010F grid.

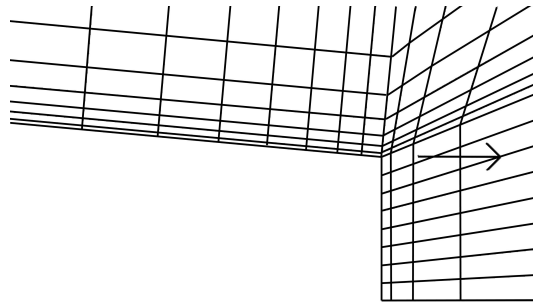


Figure 3.6: NACA 63-010F grid, detail of the flattened trailing edge. For a better grid the trailing cells should have been more aligned with the expected streamlines, indicated by the arrow

A detail of the trailing edge is displayed in Figure 3.6. The width of the cells along the side of the NACA section boundary is 0.03 mm, resulting in a wall  $y^+ = 3.4 \pm 1.0$  at  $Re = 1 \times 10^6$ . Along the flattened trailing edge, the cell width is 0.1 mm, resulting in a wall  $y^+ = 1.0 \pm 1.0$  at  $Re = 1 \times 10^6$ . For higher Reynolds numbers the cell width at the boundary was reduced to 0.003 mm, resulting in a wall  $y^+ = 2.6 \pm 0.6$  at  $Re = 1 \times 10^7$ . This permits the application of Enhanced Wall Treatment.

Figure 3.7 compares the results of the sharp trailing edge NACA 63-010 section and the flattened trailing edge NACA 63-010F section. The flattened edge results in a slightly higher drag, 90% of this increase is due to a higher pressure drag and only 10% of the increase is due to a higher viscous drag. Figure 3.8 shows several pathlines of the flow in the trailing edge region.

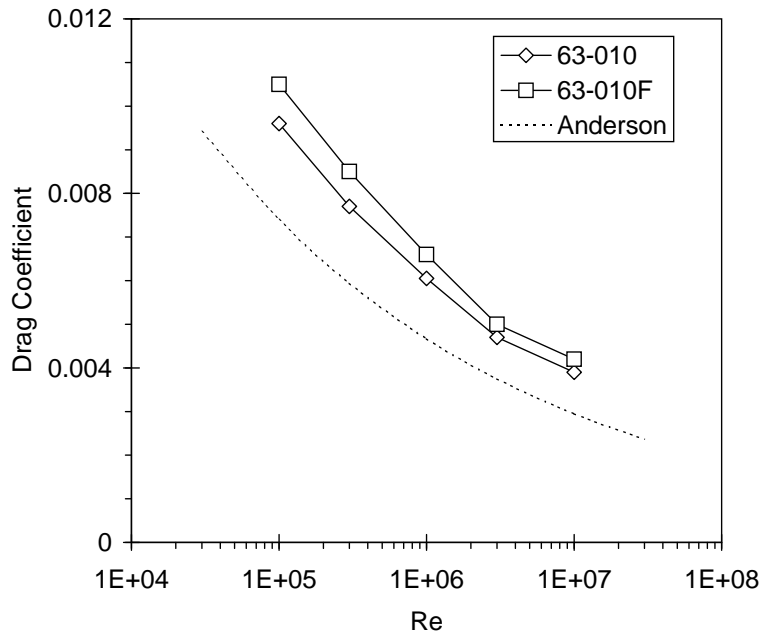


Figure 3.7: NACA 63-010F drag coefficient compared to the NACA 63-010 drag coefficient. The flattened edge appears to give an increased drag. The Anderson fully turbulent flat plate skin friction line is from Ref. [32]



Figure 3.8: Several pathlines of the flow in the trailing edge region, for  $Re = 3 \times 10^5$

### 3.4 Broken Dam

The previous problems involved only one fluid. The last two problems, the 'Broken Dam' and the 'Surface Piercing Hydrofoil,' involve two fluids: water and air. The main challenge is in computing the location of the water/air interface or 'free-surface.' These computations make use of the Volume of Fluid (VOF) method. The original paper on this method presents several benchmark problems, the 'Broken Dam' is one of them [22]: An infinitely long dam holds an amount of water 3 meters high and 1.5 meter wide. At time zero, the dam is removed and the water flows freely to the right.

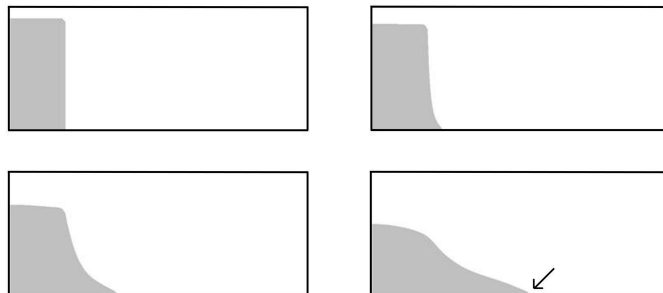


Figure 3.9: Time evolution of the free-surface for the broken dam problem. The arrow indicates the position of the waterfront as referred to in the following figure

The domain is modelled by a simple 2-dimensional rectangular grid of 640 cells. The free-surface is defined by a VOF volume fraction of 0.5. Other than previous problems, the VOF solution is time dependent. Figure 3.9 displays the time evolution of the free surface.

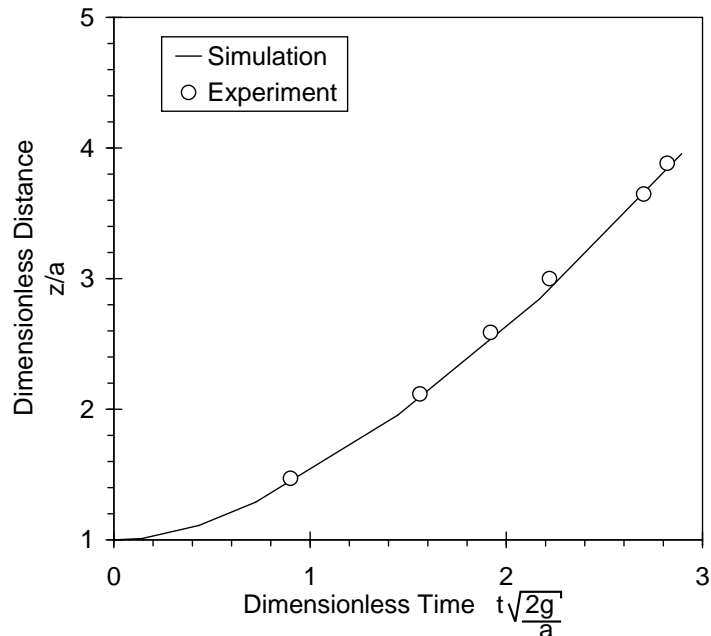


Figure 3.10: *Progress of the waterfront in time, where  $z$  is the horizontal position of the waterfront, and  $a = 1.5$  m is its original horizontal position. Experimental values from Ref. [22]*

The progress of the waterfront is compared to experimental data in Figure 3.10.

### 3.5 Surface Piercing Hydrofoil

The previous problems offered the possibility of a 2-dimensional model. This last problem is more complicated since it requires a 3-dimensional, free-surface model.



Figure 3.11: *The experimental setup of the surface piercing foil. From Ref. [34] (flipped horizontal)*

Figure 3.11 is a photograph of the experimental setup of the surface piercing foil [34]. It shows a vertically positioned NACA 0024 profile with a chord of 1.2 m, which moves horizontally through the

water at a velocity of 1.27 m/s. This situation corresponds to a Froude number of 0.37 and a Reynold's number of  $1.52 \times 10^6$ . When the flow has evolved to a steady situation, the height of the free-surface is measured at a number of positions along the profile.

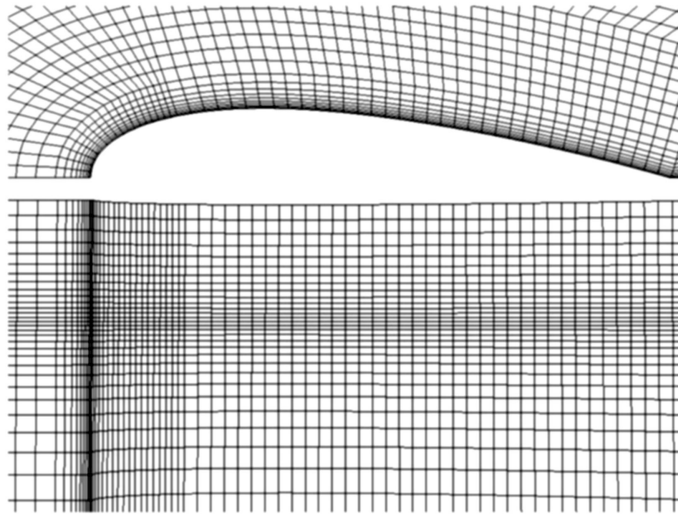


Figure 3.12: *The grid around the profile, seen from the top and seen from the side. The fluid flows in from the left*

The grid for this problem contains 118,800 cells, and is displayed in Figure 3.12. Because the problem is symmetric in the central vertical plane, I model only one half of the problem. Again, the solution is time dependent. I monitor the drag coefficient on the profile to see when the problem has reached a stationary solution. I start with a flat free-surface and run the calculations on a coarse grid. Then I use the solution of the coarse grid as an initial solution for the fine grid. For the fine grid the cell width at the NACA boundary is 1.7 mm, resulting in a wall  $y^+ = 52 \pm 17$ . This permits the application of a Standard Wall Function.

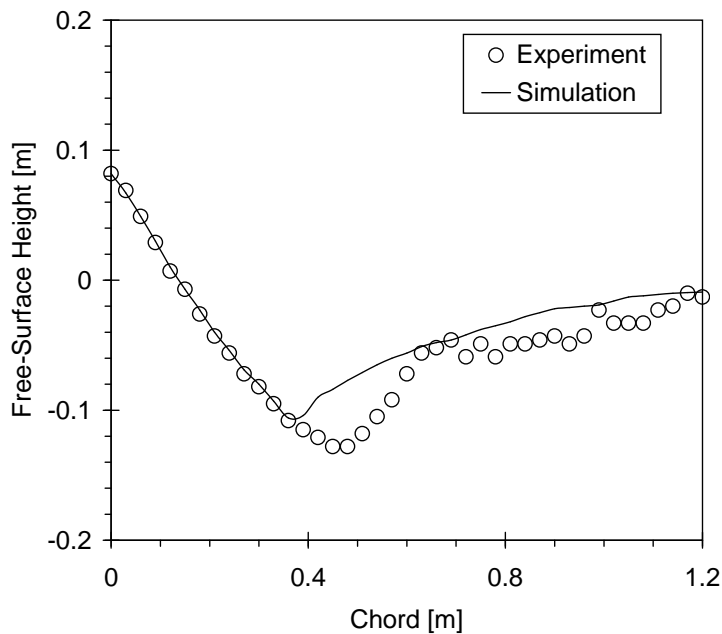


Figure 3.13: *The wave height along the profile. Experimental values from Ref. [34]*

I compare the calculated wave height along the profile to that from the experiment. As can be seen in Figure 3.13, the calculated solution is quite good except at the area around a chord of roughly 0.5 m. This is a known difficulty which is related to separation [34], an effect responsible for the development of bubbles - see Figure 3.11 - in that area.

The accuracy of the solution can be expressed by the Root Mean Squared (RMS) difference between experiment and calculation. For the coarse grid the  $\text{RMS} = 0.0225$ , for the fine grid it reduces to  $\text{RMS} = 0.0206$ . Since the solution becomes more accurate for the finer grid, one can be confident that at least part of the error could disappear on an even finer grid. However, refined grid calculations would require considerable longer CPU time and therefore are beyond the scope of these benchmark problems.<sup>3</sup>

Finally, it should be noted that the drag coefficient does not reach a steady state but appears to oscillate with a frequency of roughly 1 Hz and an amplitude of roughly 1% of the mean value. In retrospect this is probably due to having a too large time step for the finer grids.

### 3.6 Conclusions

These kind of problems offer a first rough indication of the possibilities and limitations of the computational method. Furthermore, they offer a valuable introduction to the field of Computational Fluid Dynamics. The results are promising, the main limitation is the inability to calculate the correct transition from laminar to turbulent flow.

---

<sup>3</sup>Results might improve by forcing the leading part of the flow to be laminar, thus forcing a fixed transition point. This is in fact related to the absence of a distinct drag crisis in the case of the sphere.

## Chapter 4

# 2-Dimensional Grid and Boundary Choices

Before applying the method to the full 3-dimensional sailing yacht cases, I make some choices for the grid and boundaries based on 2-dimensional simulations. Because the 2-dimensional simulations are much faster than the 3-dimensional simulations, this approach is likely to speed up the overall progress. The objective of this chapter is not to compare simulations with experimental results, but to clarify the effect of assumptions and simplifications in the simulation itself.

### 4.1 Asymptotic Range

In order to make a Richardson Extrapolation, the grids should be in the asymptotic range: a Log-Log plot of the error versus the number of grid cells should result in a straight line [25]. The hull is modeled by an axisymmetric body with the same lengthwise distribution of displacement, whereas the keel is modeled by an infinitely long wing section. The effect of the free-surface and also the interaction between the keel and the hull are of course absent in this 2-dimensional simplification. As reference values, I take the extrapolated values of very fine grids. For the hull, the wall cell width is 1.7 mm which typically results in wall  $y^+ = 59 \pm 16$ . This permits the application of a Standard Wall Function. For the keel, the wall cell width is 0.05 mm which typically results in wall  $y^+ = 2.2 \pm 1.8$ . This permits the application of Enhanced Wall Treatment.

Figures 4.1 and 4.2 are Log-Log plots of the error versus the number of grid cells along the chord. The observed convergence orders are  $p_{hull} = 2.5$  and  $p_{keel} = 2.3$ , which corresponds reasonably well with the 2<sup>nd</sup> order scheme. It can be concluded that at 16 cells over the chord both grids are in the asymptotic range. Of course, a final verification of the asymptotic range according to Formula 2.8 can be made only after the 3-dimensional simulations.

### 4.2 Turbulence Stimulation Strips

Does the  $k - \epsilon$  model invoke the same amount of turbulence as the turbulence stimulation strips? This question is addressed using the same 2-dimensional models as used in the previous section.<sup>1</sup> The turbulence strips are modeled in two different ways: by having areas with surface roughness, and alternatively by having areas with a fixed wall shear stress. Both the surface roughness and wall shear stress of the turbulence stimulation strips are known from the experiments. In order to accommodate the surface roughness, both the keel and hull wall cell width are 3 mm. For the hull this results in wall  $y^+ = 118 \pm 21$  without strips and in wall  $y^+ = 120 \pm 37$  with strips. For the keel it results in wall  $y^+ = 142 \pm 48$  without strips and in wall  $y^+ = 153 \pm 64$  with strips. This permits the application of a Standard Wall Function.

---

<sup>1</sup>The inflow velocity is 2.05 m/s instead of 1.80 m/s, since I originally intended to perform the 3-dimensional simulations at two different velocities.

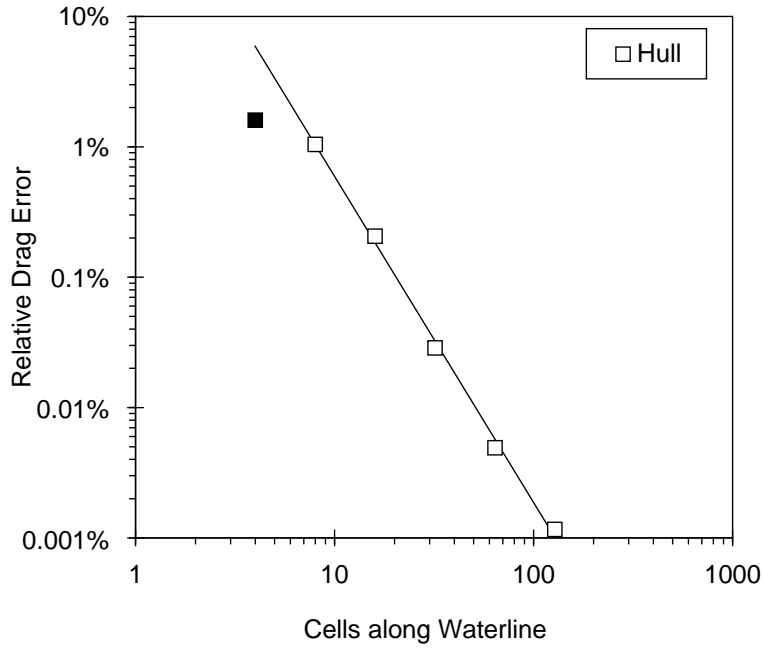


Figure 4.1: *Convergence of the hull drag for an increasing number of grid cells. A linear dependency in the Log-Log plot indicates that the grid is in the asymptotic range. The black face label is clearly out of the asymptotic range, in this case the grid is too coarse*

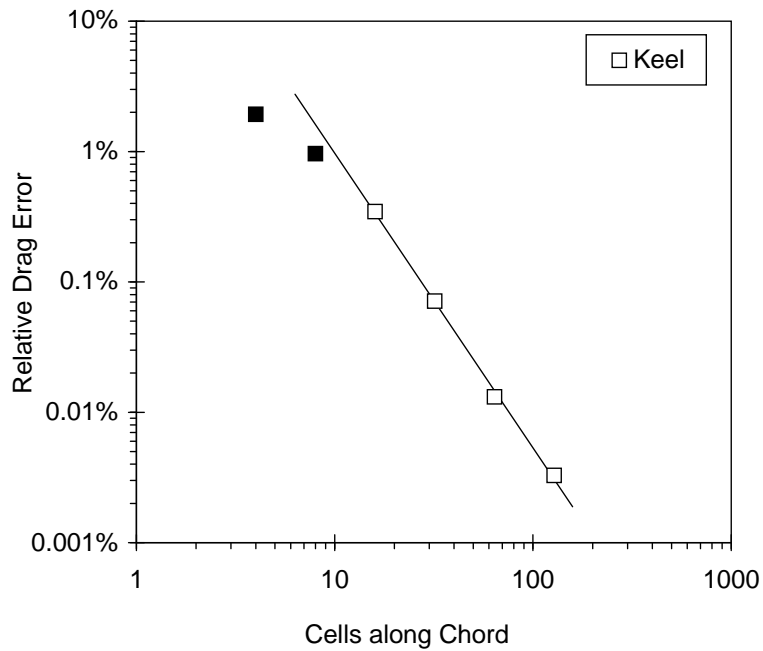


Figure 4.2: *Convergence of the keel drag for an increasing number of grid cells. A linear dependency in the Log-Log plot indicates that the grid is in the asymptotic range. The black face labels are clearly out of the asymptotic range, in these cases the grid is too coarse*

As illustrated in Figure 4.3, the surface roughness and the fixed wall shear stress have a similar effect on the turbulent intensity. Over all, the turbulence invoked by the  $k-\epsilon$  model seems appropriate.



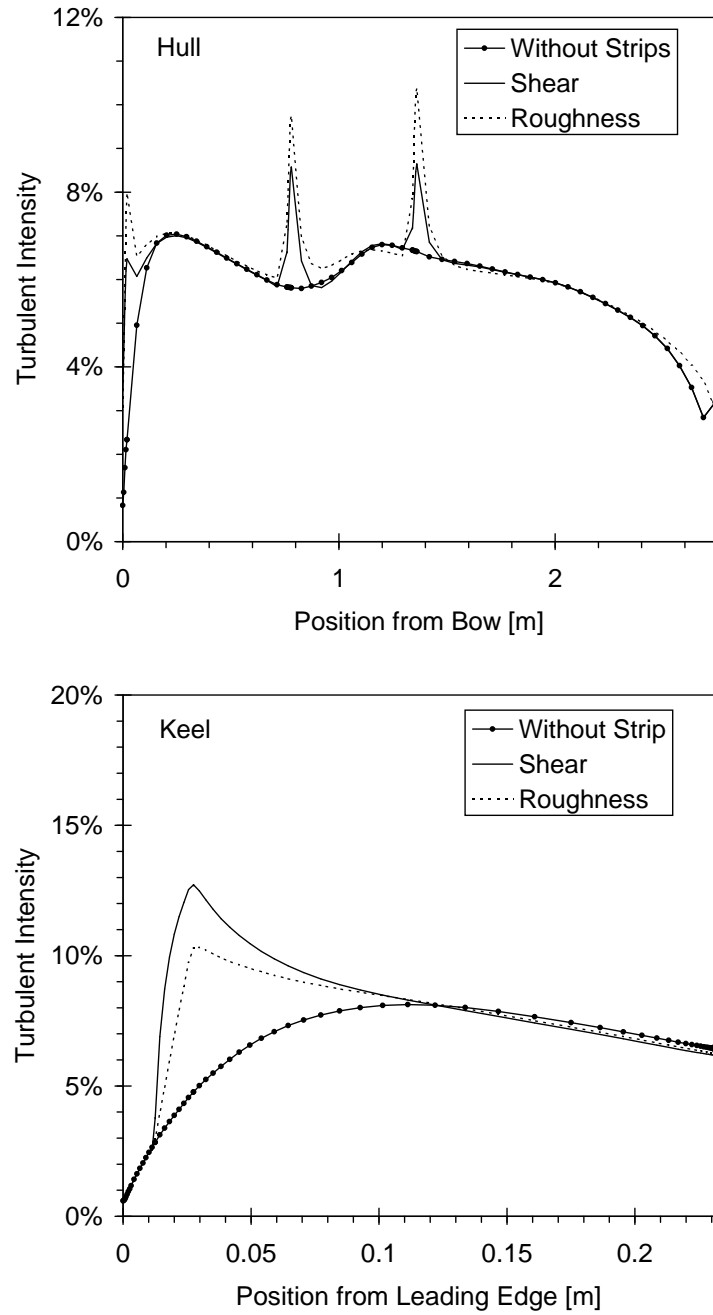


Figure 4.3: Additional effect of turbulence stimulation strips on the turbulence intensity of the hull (top) and keel (bottom)

### 4.3 Rudder Effect

What is the effect of the rudder on the keel drag? To have an indication of the order of magnitude, I model the keel and the rudder as infinitely long wing sections.<sup>2</sup> It is then possible to observe the effect of the rudder on the keel drag for various distances between both. Both the keel and rudder wall cell width are 3 mm, which results in wall  $y^+ = 138 \pm 30$  for the keel and wall  $y^+ = 135 \pm 31$  for the rudder. This permits the application of a Standard Wall Function.

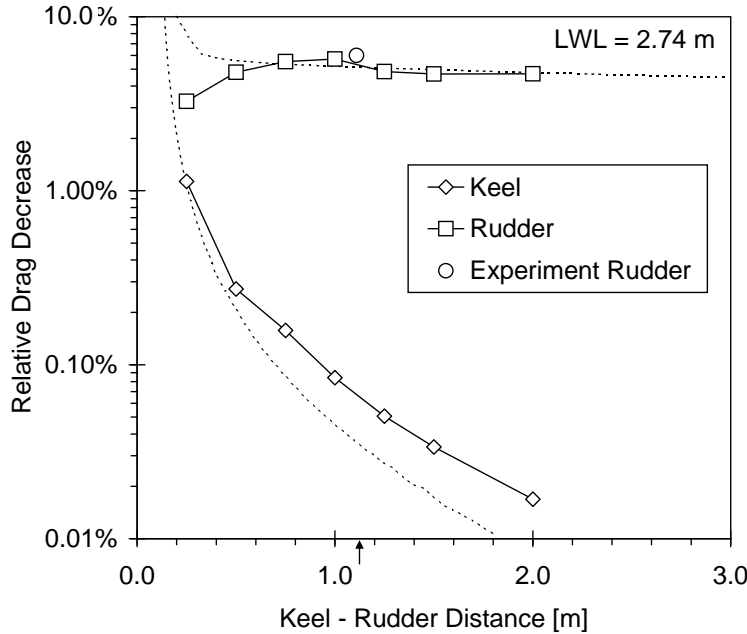


Figure 4.4: Effect of the rudder on the keel drag and vice versa. The dotted lines indicate the reduced dynamic pressure  $q$ . The arrow indicates the actual distance

As illustrated in Figure 4.4, the influence at the actual distance of 1.1 m is in the order of 0.1 %. That is, the rudder has only a minor effect on the keel drag. Figure 4.4 also indicates that the keel might have a substantial effect on the rudder drag. Finally, the lines indicate in large part the effect can be explained by the reduced dynamic pressure  $q = \frac{1}{2}\rho u^2$ , as a direct result of the reduced flow velocity  $u$ .

### 4.4 Surface Roughness

Below a certain threshold, surface roughness does not have an effect on the drag. In that case, the surface boundary condition can be considered to be a perfectly smooth wall. The surface roughness is expressed as the average grit size (*i.e.* grain size) diameter. From turbulent flat plate literature results [11], the maximum allowable keel roughness can be estimated to be 0.05 mm, while the maximum allowable hull roughness can be estimated to be 0.07 mm.

For a more specific estimate I have simulated the 2-dimensional hull and keel drag for various surface roughnesses. The hull and keel wall adjacent cell widths are 2 mm. For a surface roughness of 0.02 mm this results in wall  $y^+ = 69 \pm 17$  for the hull and in wall  $y^+ = 86 \pm 28$  for the keel. This permits the application of a Standard Wall Function. Figure 4.5 indicates that there is no drag increase up to a roughness of 0.02 mm, and that the drag increase for a roughness of 0.05 mm is still very limited. In accordance with the literature estimate, the hull is more tolerant to roughness than the keel.

<sup>2</sup>Again, the inflow velocity is 2.05 m/s instead of 1.80 m/s.

Now that the tolerable roughness is known, the next question is: How smooth is the actual surface of the ship model? In the TU Delft Ship Hydromechanics Laboratory, ship models are sandpapered and painted repeatedly. After the last paint has dried, there are still some imperfections in the surface. As a last treatment, the surface is smoothed with U.S. manufactured waterproof *Norton Aqua T223 Advance* sandpaper with a 600 CAMI grit designation. This corresponds to an average grit diameter of 0.016 mm [35], which is smaller than the tolerable 0.02 mm. This implies that the surfaces are smooth enough to be considered as perfectly smooth walls.

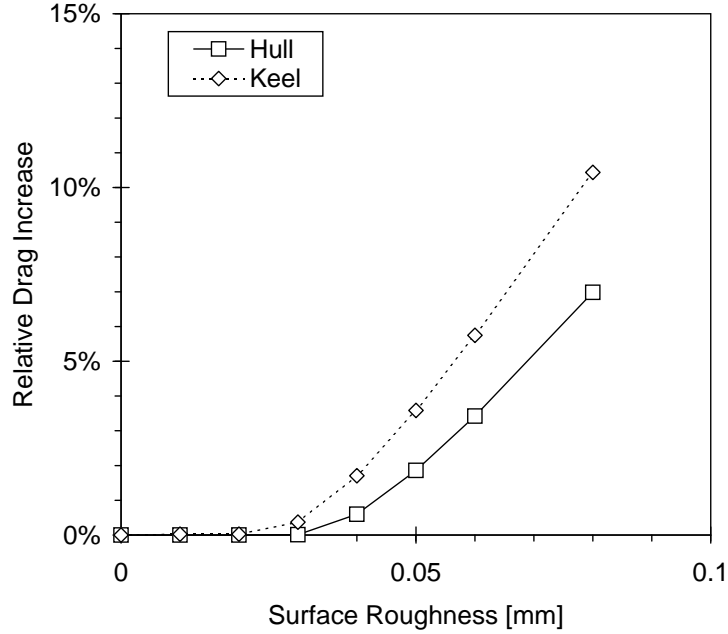
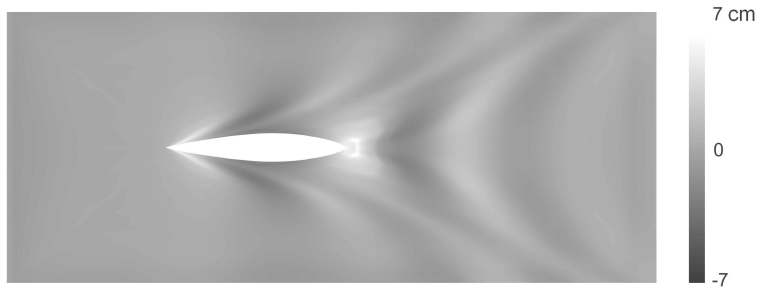


Figure 4.5: *The relative drag increase versus the surface roughness diameter. Clearly a roughness up to 0.02 mm does not effect the drag*

## 4.5 Conclusions

The grids should have at least 16 cells along the keel chord and the hull waterline in order to be in the asymptotic range. The presence of turbulence stimulation strips does not require any additional or specific simulation, other than that the  $k-\epsilon$  model is applied over the complete domain. The rudder has a negligible effect on the keel drag and can confidently be omitted from the simulation. Finally, the model surface can be considered as a perfectly smooth wall.



The calculated wave height for the bare hull at a Froude number of 0.35. The calculation of the drag of the bare hull serves as a last stepping stone, before turning to the the drag of the keel hull combination.

## Chapter 5

# Validation for the Bare Hull

In this chapter I compare simulation results for the bare hull to the experimental results. Of course this is not the actual problem of interest, however it would be desirable to be able to simulate the hull drag before adding a keel.

### 5.1 Grid

In order to make a proper grid convergence study and a Richardson Extrapolation, the problem is calculated on three different grids. The coarse grid has 16,120 cells, the medium grid has 51,408 cells and the fine grid has 199,640 cells. To give an idea, the different hulls have 38, 60, and 94 cells over the length of the ship. All grids are block structured O-grids. Figure 5.1 displays the grid on the hull, together with a midship slice perpendicular to the far field flow direction.

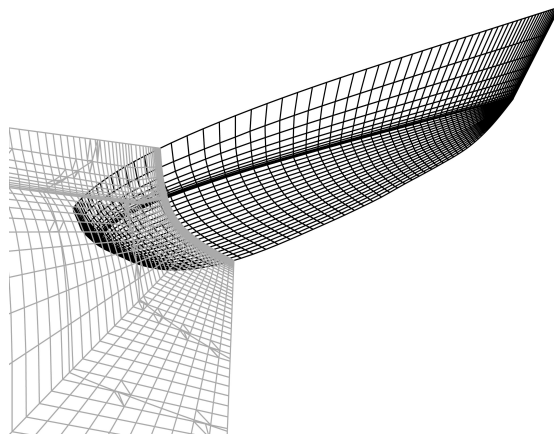


Figure 5.1: *The finest grid used for the calculation of the bare hull drag coefficient*

### 5.2 Wall $y^+$

The first cell widths along the hull are 3.6 mm for the coarse grid, 2.3 mm for the medium grid, and 1.1 mm for the fine grid. This results in a wall  $y^+$  of  $121 \pm 30$ ,  $87 \pm 29$ , and  $44 \pm 18$  respectively. This permits the application of a Standard Wall Function.

### 5.3 Time Convergence

In time, the drag coefficients tend to oscillate. After some initial wiggles, the coefficients appear to settle for a periodic behavior, with an exponentially decaying amplitude. Instead of letting the amplitude

fade out, I make a least squares fit. From that fit I determine the average value. Figure 5.2 shows the fit for the finest grid.

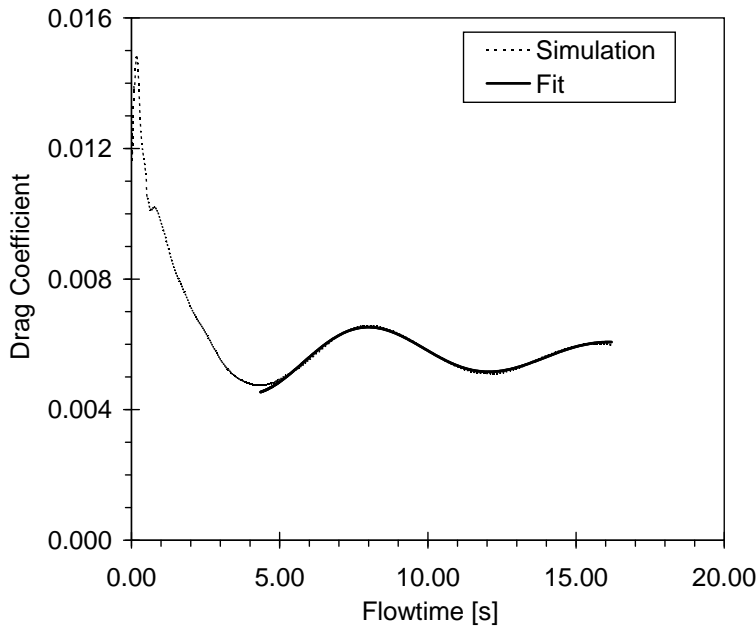


Figure 5.2: An example of the time convergence of the drag coefficient. The fit is a periodic function with an exponentially decaying amplitude

## 5.4 Grid Convergence, Richardson Extrapolation

Figure 5.3 illustrates the grid convergence for this case. The drag coefficients are plotted against the typical cell size. The observed order of the convergence is  $p = 1.89$ . The GCI ratio of Formula 2.8 is found to be 0.934, which indicates that the grids are in the asymptotic range.

The experimental drag coefficient is 0.0057 [9, 10]. The left label in Figure 5.3 indicates the extrapolated drag coefficient found in the simulation:  $0.0055 \pm 0.0006$ .

## 5.5 Conclusions

The difference between the simulated and experimental drag coefficient is smaller than the simulation error. This indicates that FLUENT gives a good estimate of the bare hull drag coefficient.

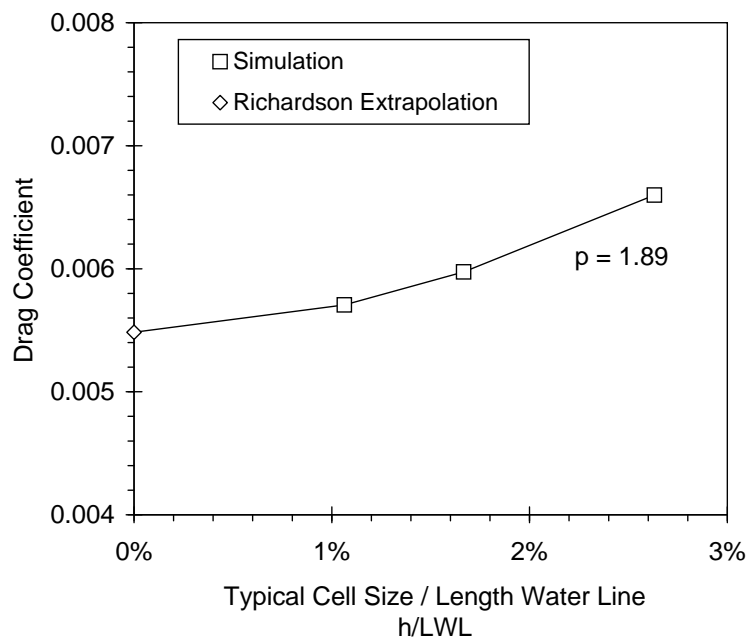
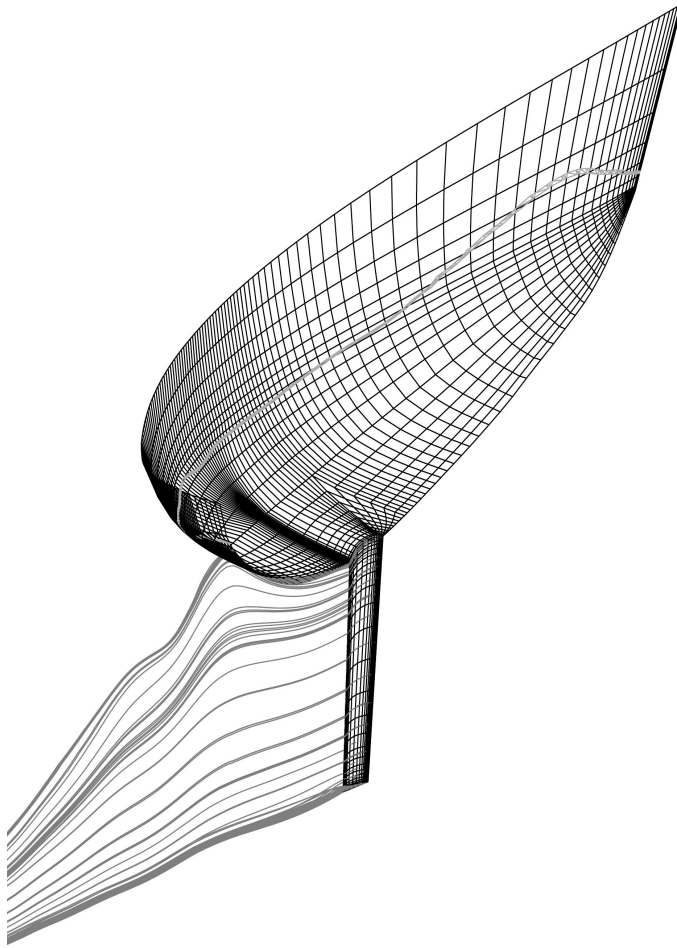


Figure 5.3: Richardson Extrapolation of the bare hull drag coefficient. The grids have an average cell length ranging from 1.1 % to 2.6 % of the ship's length. The left label indicates the extrapolated value



Pathlines traced from the Keel 1 surface, for the medium grid. Drawn from the velocity field, these pathlines are an illustration of the vast amount of physical information that results from such a 3-dimensional RANS simulation.



## Chapter 6

# Validation for the Keel Hull Combination

The model has been set up and validated for some simple cases, a number of simplifications have been motivated and verified, and the simulation showed promising results for the bare hull case. Finally everything is in place to perform the keel hull combination simulations.

For the simulation of Keel 1 I had prior knowledge of the experimental results. The simulation of Keel 3 was blind, I viewed the experimental results only after completing the simulation.

### 6.1 Grid

The problem is calculated on three different grids. For keel 1, the coarse grid has 40,512 cells, the medium grid has 136,728 cells and the fine grid has 324,096 cells. To give an idea, in the different grids the keel 1 has 16, 24, and 32 cells over the chord, thus being in the asymptotic range established in Figure 4.2. The Keel 3 case has slightly larger grids, with 24 and 32 cells over the chord in the coarse and medium grid. Figure 6.1 displays the grid for Keel 1. The 38-block structured grids are a combination of a global O-grid and a local C-grid in the  $xy$ -plane around the keel.

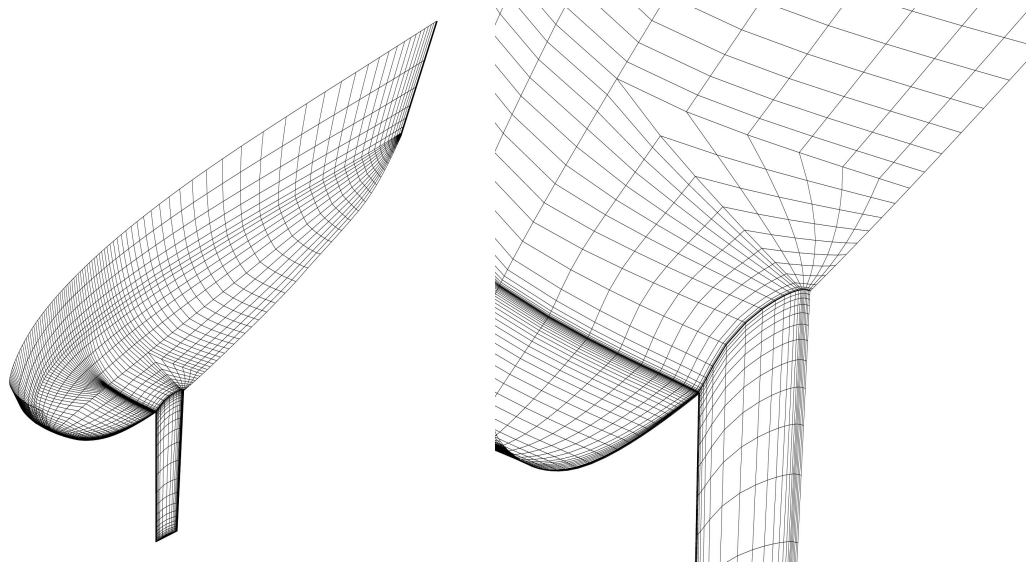


Figure 6.1: *The medium grid used for the calculation of the Keel 1 drag coefficient. The detail on the right illustrates the C-grid around the keel and the high cell density at the trailing edge*

## 6.2 Wall $y+$

The keel trailing edge is a challenge for proper grid generation. It requires much smaller grid cells than the remaining domain. Therefore I have chosen to have the first layer of cells at the keel side in the viscous sublayer (wall  $y+ < 5$ ) and at the same time have the first layer of cells at the hull and the keel bottom in the Logarithmic layer ( $30 < \text{wall } y+ < 300$ ). This is enabled by FLUENT's Enhanced Wall Treatment, since it is a blended model [14]. The cell widths and resulting wall  $y+$  are shown in Table 6.1.

Table 6.1: *First cell width and wall  $y+$*

keel	grid	width			wall $y+$		
		hull	keel side	keel bottom	hull	keel side	keel bottom
1	coarse	3.0 mm	0.050 mm	4.0 mm	$92 \pm 27$	$2.3 \pm 0.7$	$161 \pm 21$
1	medium	2.0 mm	0.033 mm	2.7 mm	$76 \pm 24$	$1.6 \pm 0.7$	$121 \pm 14$
1	fine	1.5 mm	0.025 mm	2.0 mm	$61 \pm 24$	$1.3 \pm 0.8$	$96 \pm 10$
3	coarse	6.0 mm	0.120 mm	6.0 mm	$201 \pm 54$	$3.7 \pm 1.2$	$125 \pm 4$
3	medium	4.0 mm	0.120 mm	4.0 mm	$133 \pm 33$	$3.8 \pm 1.4$	$93 \pm 4$

## 6.3 Time Convergence

The keel drag coefficient converges rapidly in time, whereas for Keel 1 the hull drag coefficient oscillates. In the same manner as in Figure 5.2 I have made a least squares fit to determine the average value. However, for the Keel 3 case I used a different iteration sequence that resulted in a properly converging drag, shown in Figure 6.2. Because the hull drag coefficient converges much slower than the keel drag coefficient, I have opted to converge the coarse and medium grid for both coefficients and converge the fine grid for the Keel 1 drag coefficient only. I then use the bare hull convergence order for the hull drag coefficient Richardson Extrapolation.

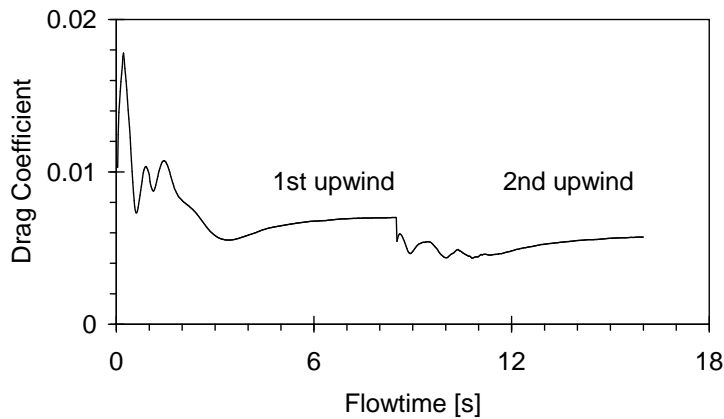


Figure 6.2: *Example of the time convergence of the hull drag for the Keel 3 case*

## 6.4 Grid Convergence, Richardson Extrapolation

Figure 6.3 illustrates the grid convergence for Keel 1. The drag coefficients are plotted against the typical cell size. The observed order of the convergence for the Keel 1 drag coefficient is  $p = 1.85$ . The GCI ratio (Formula 2.8) is found to be 0.992 for Keel 1, which indicates that the grids are the asymptotic range.

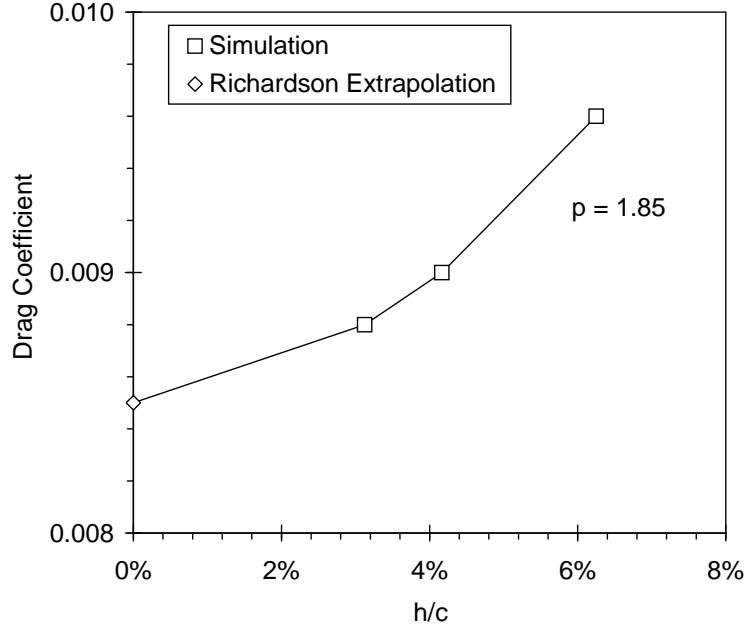




Figure 6.3: *Richardson Extrapolation of the Keel 1 drag coefficient. The different grids have an average cell length ranging from 3% to 7% of the keel's chord. The grey faced label indicates the extrapolated value with error bars*

Together with the bare hull results of the previous chapter, the resulting hull and keel drag coefficients are displayed in Table 6.2. Note that the convergence order in brackets is taken from the bare hull simulation and that the convergence order in square brackets is taken from Keel 1.

Table 6.2: *Drag Coefficients: The values observed in the simulation compared to the experimental values. The last column indicates the validity of the simulation, where A indicates that the difference between simulation and experiment is within half the error, B indicates that the difference is within the error, and C indicates that the difference is larger than the error*

keel	planform	surface	observed convergence order	present simulation	experiment [9, 10]	offset	valid
none		hull	1.89	$0.0055 \pm 0.0006$	0.0057	-4%	A
1		hull	(1.89)	$0.0057 \pm 0.0004$	0.0058	-3%	A
		keel	1.85	$0.0085 \pm 0.0008$	0.0091	-7%	B
3		hull	(1.89)	$0.0061 \pm 0.0006$	0.0055	10%	C
		keel	[1.85]	$0.0074 \pm 0.0010$	0.0071	5%	A

## 6.5 Wave Height

The simulation results in a certain wave pattern. Although it is not the main objective of the simulation, it would be nice to compare the wave height along the hull with the experimental results. However, these experimental results are not available for this case. Therefore Figure 6.4 compares the present results with the results from a potential flow simulation for the same case.

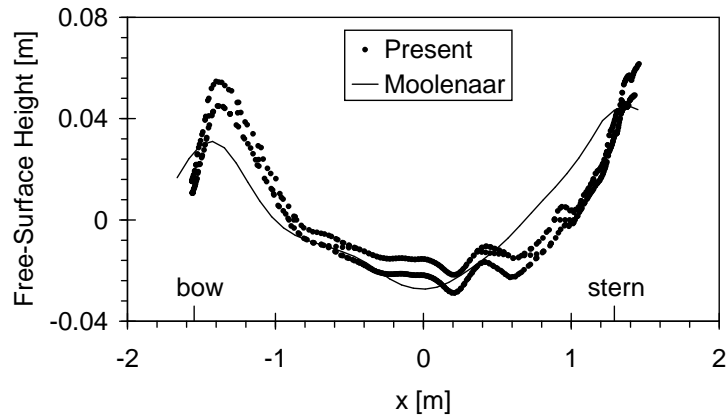
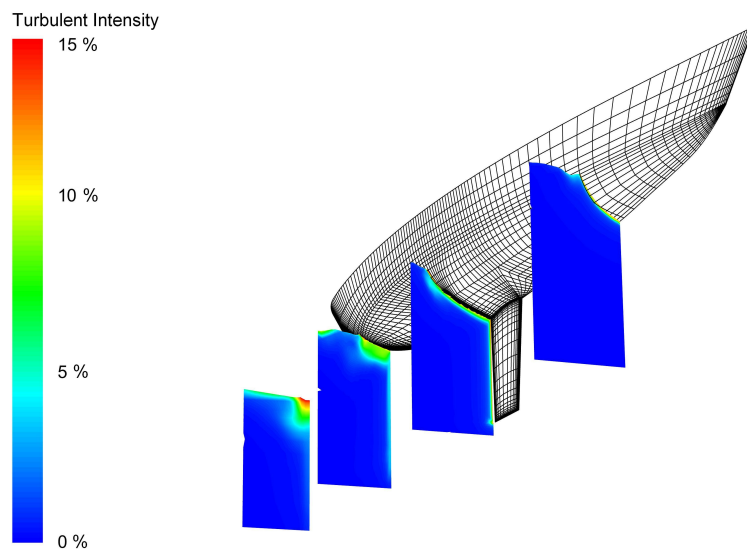
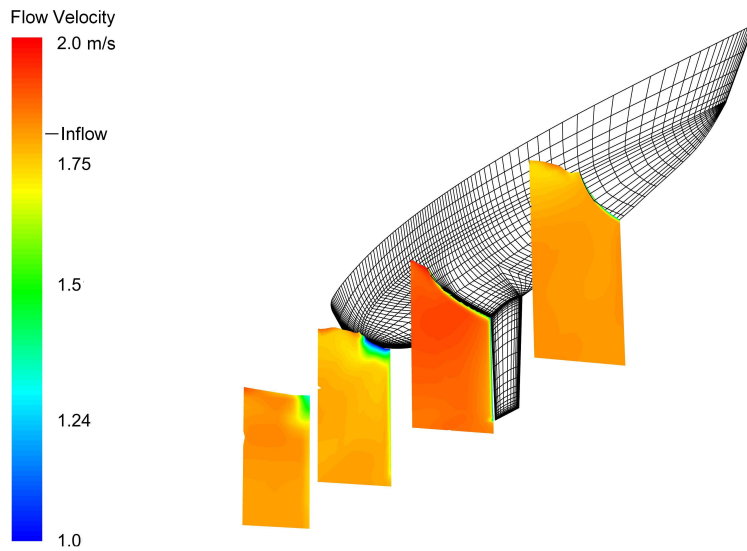


Figure 6.4: Comparison of the free-surface height along the hull, taken from the present Keel 1 simulation and from a potential flow simulation. The present data is for a VOF fraction from 0.4 to 0.6. The potential flow results by Moolenaar are from Ref. [36, 37]

## 6.6 Conclusions

Three drag coefficients are in excellent agreement with the experimental results, two are in good agreement and one is in poor agreement. In general, the coefficients are within 10% of the experimental results.





Slices at different lengthwise positions, where the colors indicate the flow velocity (top) and turbulent intensity (bottom). The slices show a distinct effect of the keel and hull wake.

# Chapter 7

## Practical Implications

Although the simulations are not completely validated, I propose some methods that could give better understanding of some mechanisms involved. I consider the interaction between keel and rudder, the scaling of this interaction, and the scaling of the keel drag. For this chapter the amount of simulation details (convergence, wall  $y+$ , etc.) is so large that I have decided to place it in an Appendix.

### 7.1 Keel Rudder Interaction

From experiments the keel is known to have a substantial effect on rudder performance. In the keel wake, the rudder experiences a reduced flow velocity and an increased turbulent intensity. Here I look at the effect of changing the rudder position and of changing the Froude number. I average the flow velocity reduction and turbulent intensity over a rectangular envelope enclosing the rudder, positioned perpendicular to the far field velocity.

The position of the rudder, and thus the distance behind the trailing edge of the keel, has an effect on the velocity reduction and the turbulent intensity experienced by the rudder. Figure 7.1 shows that the velocity reduction due to the bare hull may constitute a substantial part of the total velocity reduction. The turbulent intensity can be seen to originate almost completely from the keel.

A different ship speed might change this keel and hull wake. Instead of changing the ship speed, I have changed the Froude number and Reynold's number accordingly by means of a different gravity and viscosity. Since - by dimensional analysis - the flow is characterized by the Froude number and Reynold's number, this leads to the same results [11, 12]. For these simulations the rudder is in the actual rudder position ( $D = 1.11$  m). Figure 7.2 illustrates that the ship speed has an effect on the velocity reduction, but has hardly any effect on the turbulent intensity.

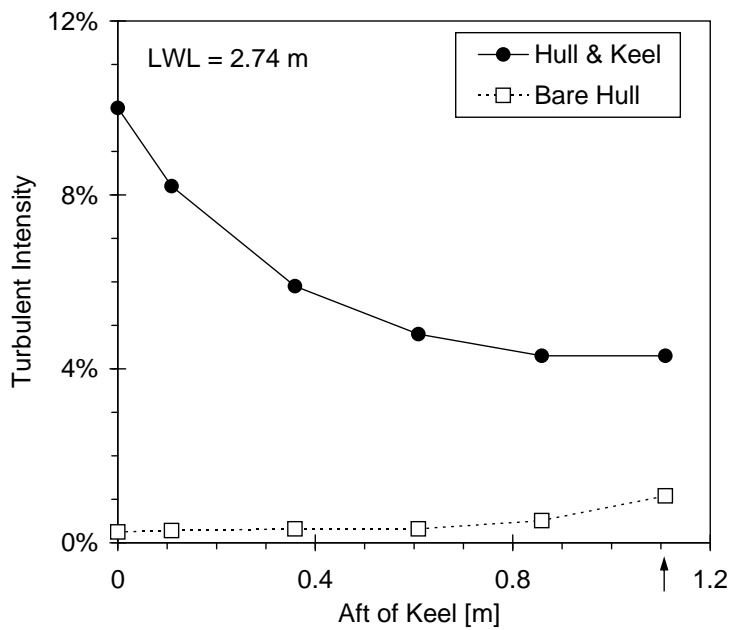
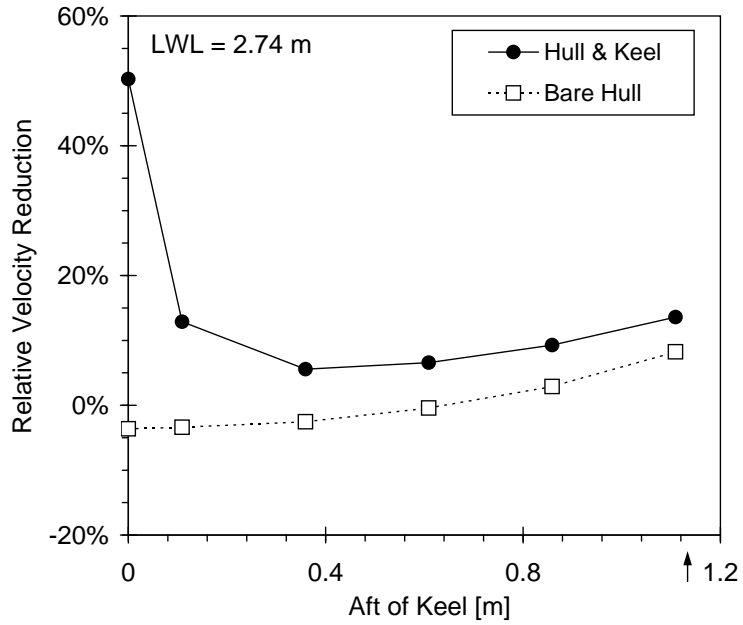


Figure 7.1: The velocity reduction and turbulence experienced by the rudder, as a function of the rudder distance behind the trailing edge of the keel. The arrow indicates the actual rudder distance



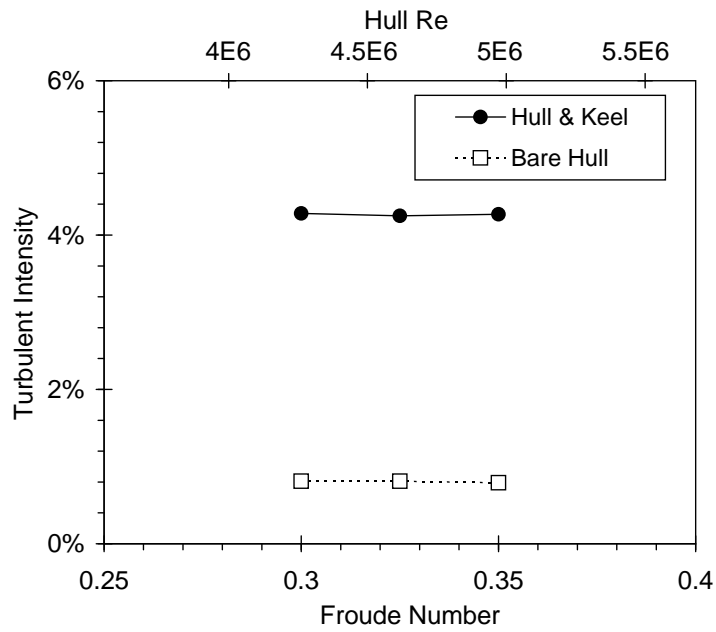
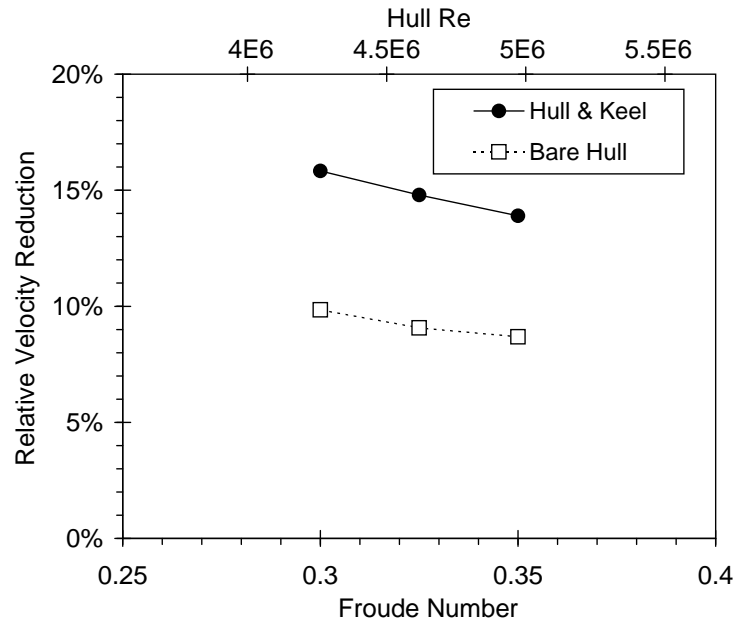


Figure 7.2: The velocity reduction (top) and turbulence (bottom) experienced by the rudder for different Froude numbers. The Reynold's number has been scaled accordingly

## 7.2 Scaling Keel Rudder Interaction

Towing tank experiments rely on the assumption that the effects can be scaled by either the Froude number or the Reynold's number [12, 13]. Due to the setup of the experiment - where the experimental and full scale Froude number are equal - it would be desirable to have the keel rudder interaction scale with the Froude number.

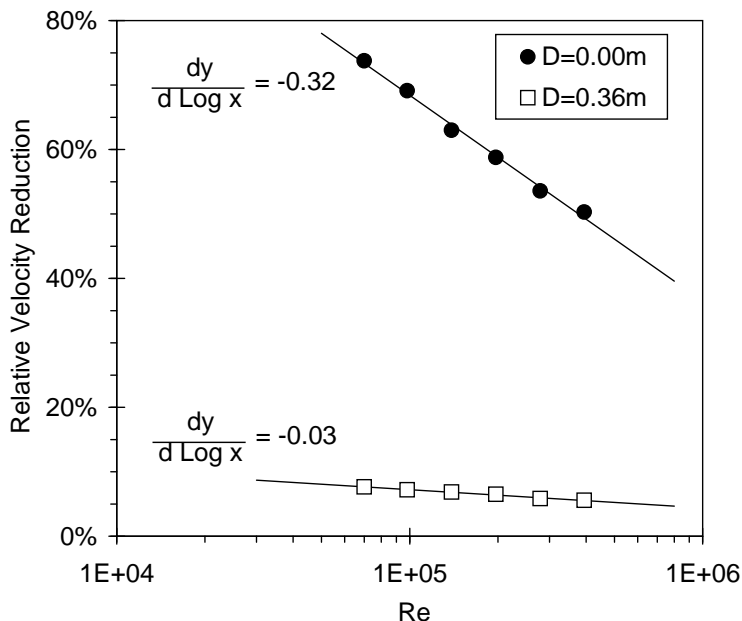


Figure 7.3: The Reynold's number dependency of the velocity reduction at two different positions behind the keel trailing edge. The resulting slopes are displayed in the following figure. Typically  $Re_{model} = 4 \times 10^5$  and  $Re_{full\ scale} = 7 \times 10^6$

I have changed the Reynold's number by means of a different viscosity,<sup>1</sup> and then analyzed the keel rudder interaction. As an example Figure 7.3 displays the Reynold's number dependency of the velocity reduction experienced by the rudder, for two different rudder positions. It shows that, were the rudder to be positioned directly at the keel trailing edge, the velocity reduction would change severely with a changing Reynold's number. For a larger keel rudder distance, this dependency is smaller. I have quantified this dependency by taking the slope:

$$\frac{\partial \left(1 - \frac{u}{u_\infty}\right)}{\partial \text{Log}(Re)} \quad (7.1)$$

The resulting slopes are displayed in Figure 7.4. It is clear that close to the keel trailing edge the wake depends on the Reynold's number, while at the actual experimental rudder position ( $D = 1.11\text{ m}$ ) there is hardly any dependence. For normal rudder positions, the keel rudder interaction can confidently be taken to be Froude scaled.

<sup>1</sup>I choose to increase the viscosity, thereby lowering the Reynold's number. A higher Reynold's number would have been less likely to lead to a converging simulation.

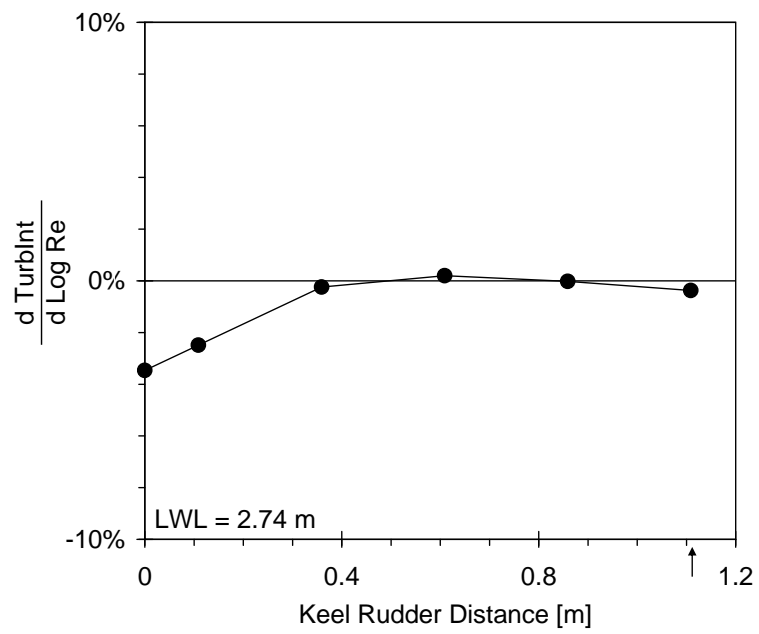
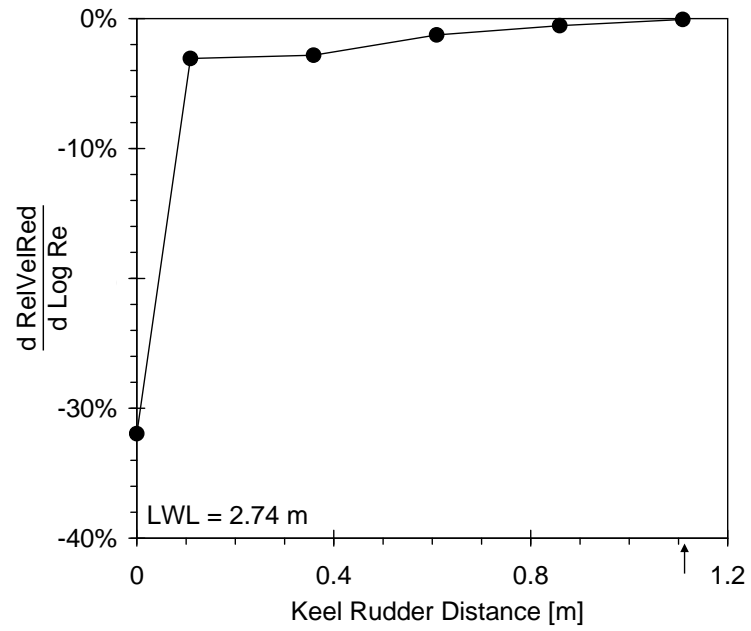


Figure 7.4: The effect of a different Reynold's number on the velocity reduction (top) and the turbulent intensity (bottom). The slopes are determined as in the previous figure. The arrow indicates the actual distance

### 7.3 Scaling Keel Drag

The keel drag is scaled by means of the form factor method, which relies on the assumption that the total keel drag coefficient  $C_T$  depends on the residuary keel drag coefficient  $C_{Res}$ , the form factor  $(1+k)$ , and the skin friction coefficient<sup>2</sup>  $C_F$  as [12]:

$$C_T = C_{Res} + (1+k)C_F \quad (7.2)$$

By changing the Reynold's number by means of a different viscosity, I can verify this dependency for the current simulation. Plotting  $C_T$  against  $C_F$  should show a linear dependency. Figure 7.5 shows the simulated values with a linear fit. The correlation coefficients are 0.990 for Keel 1 and 0.994 for Keel 3. This supports the assumption that the form factor method can be applied.

For practical application of the form factor method, it is important to know how the skin friction should be scaled. Among several options, there are two main candidates. The first is the ITTC-57 ship correlation line intended for free-surface ship hulls [13]:

$$C_F^{ITTC} = \frac{0.075}{[\text{Log}(Re) - 2]^2} \quad (7.3)$$

The second is the turbulent flat plate skin friction line by Anderson [32, 33]:

$$C_F^{And} = \frac{0.074}{Re^{1/5}} \quad (7.4)$$

Figure 7.6 shows the simulated results together with both these lines. To apply the form factor method successfully, for each keel the ratio of the simulated skin friction and these lines should be constant. Figure 7.7 shows these ratios for the present data. The Anderson flat plate skin friction line leads to more constant ratios than the ITTC-57 ship correlation line. Although the error margins are quite large, this might be an indication that for the scaling of the keel drag the Anderson line is more suitable than the ITTC-57 line.

### 7.4 Conclusions

The hull and keel wake are characterized by the reduced flow velocity and the turbulent intensity. The simulations show a distinct wake of the hull and keel at the rudder position. The wake depends on the rudder position and on the Froude number. Close to the keel trailing edge the wake depends on the Reynold's number, for larger keel rudder distances the wake does not and is therefore Froude scaled.

The simulations support the assumption that keel drag can be scaled by means of the form factor method. To scale the skin friction drag, the Anderson flat plate correlation line might be more suitable than the ITTC-57 ship correlation line.

---

<sup>2</sup>This is the total skin friction coefficient  $C_F$ , different from the local skin friction coefficient  $c_f$

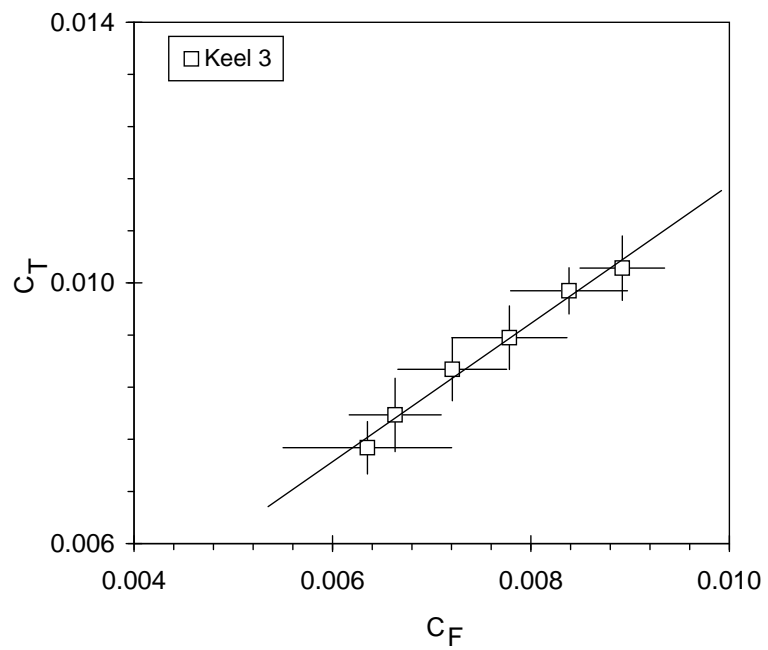
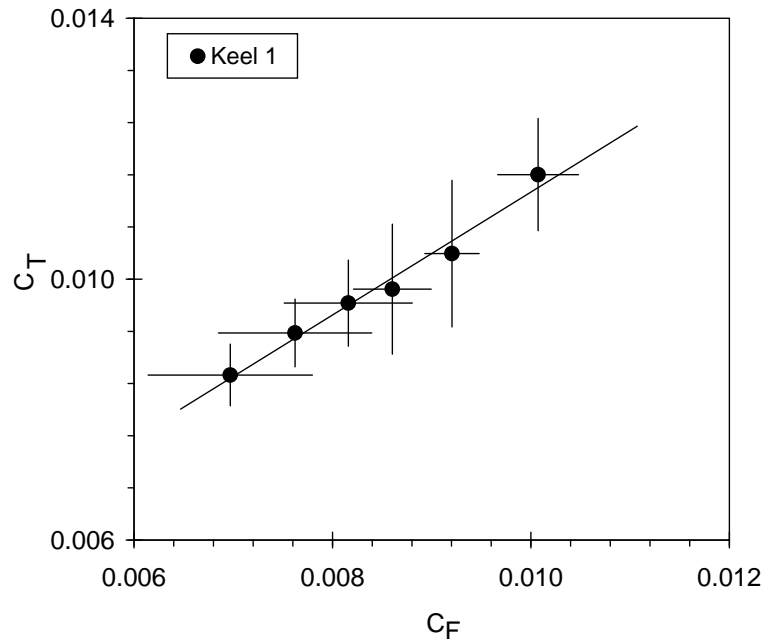


Figure 7.5: *The total drag versus the skin friction. Application of the form factor method relies on a linear dependency of these variables*

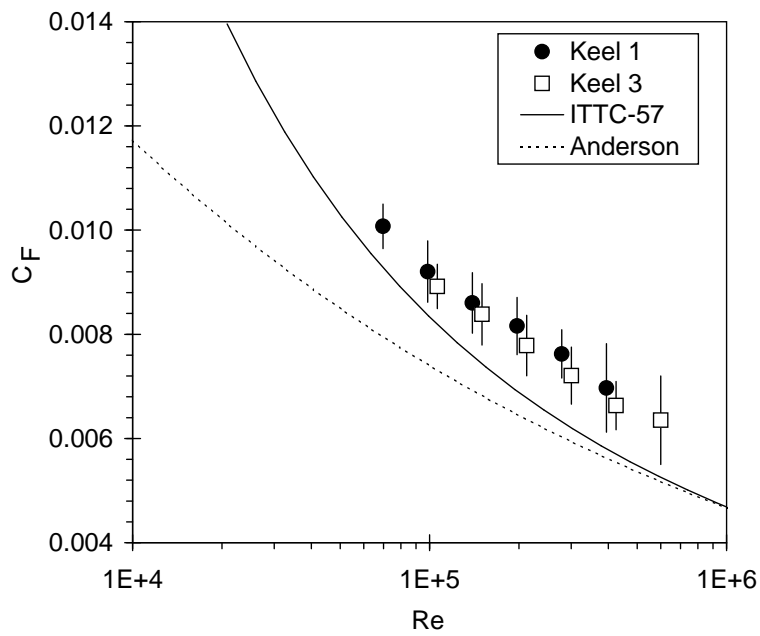


Figure 7.6: The skin friction compared to the ITTC-57 ship correlation line [13] and the Anderson turbulent flat plate friction line [32]. Typically  $Re_{model} = 4 \times 10^5$  and  $Re_{full\_scale} = 7 \times 10^6$

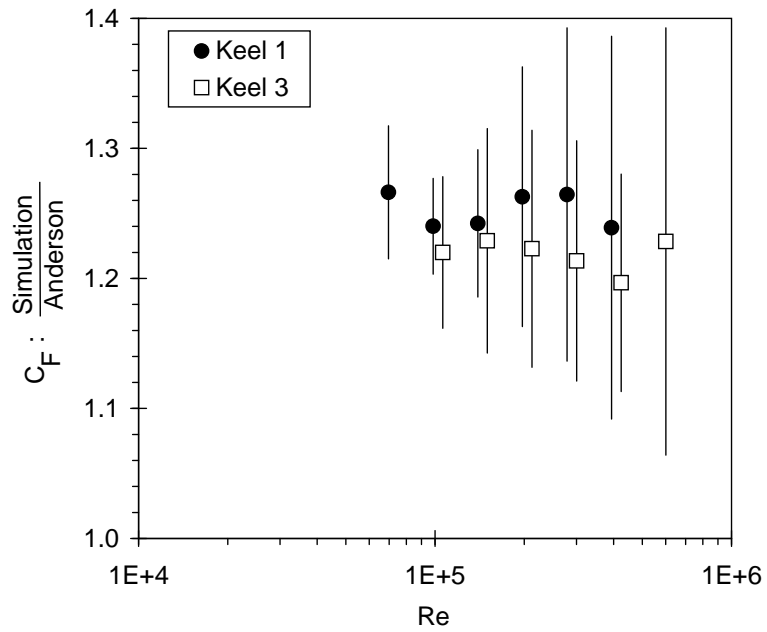
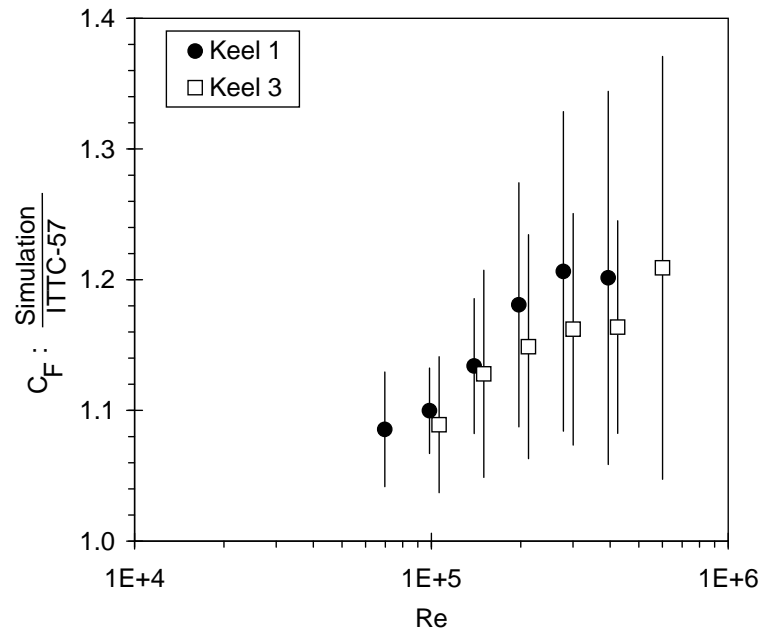


Figure 7.7: The observed skin friction divided by: the ITTC-57 Ship Correlation Line [13] (left), and divided by the Anderson turbulent flat plate friction line [32] (right). The form factor method relies on a constant value of these ratios for each keel. Typically  $Re_{model} = 4 \times 10^5$  and  $Re_{full\_scale} = 7 \times 10^6$

The SWOT analysis was originally designed as a tool for Marketing Strategy [38]. It has now found its way into other disciplines, such as Sport Psychology. First it identifies the main goal of the simulation. Then it observes the internal strengths and weaknesses of the simulation (*i.e.* method, grid, and solver). Finally, it discusses external opportunities and threats that might effect future simulations.



# Chapter 8

## Discussion

The main goal of the simulations is to provide reliable estimates of the drag coefficients of keel hull configurations. The present study indicates that FLUENT can give reliable estimates. The difference between the simulation drag results and the experiment was within the error margin for four out of five drag coefficients obtained. In general, the simulation drag results are within 10% of the experimental results.

The simulations indicate that the keel rudder interaction is Froude scaled, that the keel drag can be analyzed with the form factor method, and that the Anderson flat plate skin friction line might be more appropriate to do so than the ITTC-57 ship correlation line.

### 8.1 Strengths

STRUCTURED GRID. All the simulations are run on structured grids. This is associated with faster convergence and more reliable results [7]. Also it facilitates a better representation of the boundary layer. I have not encountered any other application of a structured grid (*i.e.* without triangular cells) for a keel hull configuration.

WALL  $y^+$ . I have taken much care to have all the grids in the proper range of wall  $y^+$ . Even more, the values are often close to the most desirable 1 (viscous sublayer) or 30 (Log layer).

GRID CONVERGENCE STUDY. The verification of the asymptotic range combined with simulations on two or three grids lead to a proper GCI grid convergence study. The observed 3-dimensional convergence orders are near the discretization order of two.

ERROR MARGIN. The GCI grid convergence study at the same time provides an extrapolated drag coefficient together with an error margin. Without this study, it would not have been possible to determine objectively if the estimated drag coefficients are within an acceptable margin of error.

### 8.2 Weaknesses

TURNOVER TIME. The turnover time of the simulations is far too long. If it was lower, I could have run the simulation for more cases.

FREE-SURFACE DISTORTION. For the keel hull combinations, the grid cell size growth might lead to distortion of the free-surface. There appears to be a trade off. The distortion appears for the present VOF Geometric Reconstruction scheme, while the distortion does not appear for other VOF schemes like 'Quick' - which then however give an overly smudged free-surface.

TURBULENCE STIMULATION. At the end of my project, I have reconsidered the results in Figure 4.3, concerning the added turbulence intensity due to the turbulence stimulation strips. Although the decay of the turbulence seems to happen in a natural fashion, I now have some doubts about the effect the

added turbulence has on the drag coefficient. More precisely, I now think that the assumption that no turbulence stimulation is needed in the simulation is correct for the hull but not for the keel. For the 2-dimensional case, I have evaluated the added drag due to the turbulence stimulation strips. For the hull it is in the order of -0.5%, whereas for the keel it is in the order of 5%. This might be an important factor, recommendable for future research.

GRID. Although the grids are found to be in the asymptotic range, I would suggest to use finer grids for future simulations. The problem is that a coarser grid will lead to higher grid growth factors and also to a smaller number of cells in the boundary layer.

### 8.3 Opportunities

BETTER GRID GENERATION. More specialized grid generators are (becoming) available, facilitating better and faster block structured grid generation.<sup>1</sup>

OPEN CHANNEL FLOW. Fluent 6 does not facilitate the correct boundary conditions for open channel flow, however in Fluent 12 the correct settings should be available. This would enable running a time steady simulation.

MACHINE IMPROVEMENTS. Improvements in machine capacity and speed are likely to decrease future simulation turnover time.

AMOUNT OF VALIDATION DATA. The amount of validation data at the TU Delft is overwhelming. Reference [9] alone contains over 50 cases, of which I have studied three.

### 8.4 Threats

BIAS. While setting up a simulation one can become biased by the experimental results known *a priori*. For future research it might be considered to do a larger number of 'blind' simulations, with *a posteriori* knowledge of the experimental results.

UNJUSTIFIED CONFIDENCE. One might be inclined to be convinced by such simulations too hastily. Each CFD application requires proper validation of a similar case.

---

<sup>1</sup>Like ICEMCFD, which gives far nicer results [7, 39].

### Acknowledgments

My gratitude goes out to Mr Huijsmans, Mr Keuning, Mr Pourquoi, and Mr Gerritsma for their enthusiasm and guidance during this project and for their stimulating lectures in previous years. I would like to thank Michiel Katgert and Ralph Moolenaar for kindly sharing their ideas and their data. I would like to thank the *cfD-online.com* community for their repeated assistance. I would like to thank Claire Evans for translating the Multatuli text. I am very thankful to Hein de Baar, Nienke de Baar, Sadok Lamine, Jacqueline Dees, and Marleen Maassen for all their suggestions and proofreading.

I would like to thank my parents and Nienke, Laura, and Yke for all of their support. I would especially like to thank my grandparents, who provided a welcoming home during the first weeks of this project. I have good memories of visits to the HISWA and to Conyplex with Mr Conijn and also of the discussions on yachting with Mr Meriwani during our sailing trips, both of which have encouraged my fascination for sailing yacht design. I am very thankful for the assistance by Mr Kupka and his staff.

# Bibliography

- [1] B. Stannard. *The Triumph of Australia II - The America's Cup Challenge of 1983*. Lansdowne, 1983.
- [2] M. Peters. *Computational Fluid Dynamics for Sport Simulation*. Springer-Verlag, 2010.
- [3] M. Estivalet and P. Brisson. *The Engineering of Sport 7*. Springer-Verlag, 2008.
- [4] N. Caplan, A. Coppel, and T. Gardner. A review of propulsive mechanisms in rowing. *Proceedings of the Institution of Mechanical Engineers, Part P: Journal of Sports Engineering and Technology*, 224:1–8, 2010.
- [5] Y. Tahara, J. Longo, and F. Stern. Comparison of CFD and EFD for the Series 60  $C_B = 0.6$  in steady drift motion. *J. Mar. Sci. Technol.*, 7:17–30, 2002.
- [6] Y. Tahara, R.V. Wilson, P.M. Carrica, and F. Stern. RANS simulation of a container ship using a single-phase level-set method with overset grids and the prognosis for extension to a self-propulsion simulator. *J. Mar. Sci. Technol.*, 11:209–228, 2006.
- [7] D. Detomi, N. Parolini, and A. Quarteroni. Numerical models and simulations in sailing yacht design. In M. Peters, editor, *Computational Fluid Dynamics for Sport Simulation*, pages 1–31. Springer-Verlag, 2010.
- [8] J.A. Keuning and B.J. Binkhorst. Appendage resistance of a sailing yacht hull. *Chesapeake Sailing Yacht Symposium*, 1997.
- [9] J.A. Keuning, M. Katgert, and K.J. Vermeulen. Keel-rudder interaction on a sailing yacht. *19th International HISWA Symposium on Yacht Design and Yacht Construction*, 2006.
- [10] M. Katgert. Private communication. 2009.
- [11] F.M. White. *Fluid Mechanics*. McGraw-Hill, 2008.
- [12] V. Bertram. *Practical ship hydrodynamics*. Butterworth-Heinemann, 2000.
- [13] M.L. Acevedo and L. Mazarredo. *Eight International Towing Tank Conference – Proceedings*. ITTC Madrid, 1957.
- [14] ANSYS. *FLUENT 6.3 User's Guide*, 2006.
- [15] B. Mohammadi and O. Pironneau. *Analysis of the k-epsilon Turbulence Model*. Wiley, 1993.
- [16] J. van Kan, A. Segal, and F. Vermolen. *Numerical Methods for Scientific Computing*. VSSD, 2005.
- [17] N. Parolini. *Computational Fluid Dynamics for Naval Engineering Problems (PhD Thesis)*. EPFL, 2004.
- [18] T.-H. Shih, W.W. Liou, A. Shabbir, Z. Yang, and J. Zhu. A new k- $\epsilon$  eddy viscosity model for high Reynold's number turbulent flows. *Computers & Fluids*, 24:227–238, 1995.
- [19] J.-Y. Kim, A.J. Ghajar, C. Tang, and G.L. Foutch. Comparison of near-wall treatment methods for high Reynold's number backward-facing step flow. *Int. J. of Comp. Fluid Dynamics*, 19:493–500, 2005.
- [20] P.A. Durbin. On the k-3 stagnation point anomaly. *International Journal of Heat and Fluid Flow*, 17(1):89 – 90, 1996.
- [21] D.E. Coles and E.A. Hirst. Computation of turbulent boundary layers. *AFOSR-IFP-Stanford Conference, Vol. II, Stanford University*, 1969.
- [22] C.W. Hirt and B.D. Nichols. Volume of fluid (VOF) method for the dynamics of free boundaries. *J. Comp. Phys.*, 39:201–225, 1981.
- [23] Clay Mathematics Institute. <http://www.claymath.org/millennium/>, 2000.
- [24] D. Ang, L. Chen, and J. Tu. Unsteady RANS simulation of high Reynold's number trailing edge flow. *15th Australasian Fluid Mechanics Conference*, 2004.
- [25] P.J. Roache. *Verification and Validation in Computational Science and Engineering*. Hermosa Publishers, 1998.
- [26] S.Y. Wang. *Verification and validation of 3D free-surface flow models*. American Society of Civil Engineers, 2009.
- [27] P.P. Brown and D.F. Lawler. Sphere drag and settling velocity revisited. *J. Envir. Engrg.*, 129:222–231, 2003.
- [28] D.A. Jones and D.B. Clarke. *Simulation of Flow Past a Sphere using the Fluent Code*. Defence Science and Technology Organisation (Australia), DSTO-TR-2232, 2008.
- [29] H.E. Donley. The drag force on a sphere. *UMAP Journal*, 12(1):47–80, 1991.
- [30] H.E. Donley. Private communication. 2009.
- [31] I.H. Abbott and A.E. von Doenhoff. *Theory of Wing Sections*. Dover Publications New York, 1959.
- [32] J.D. Anderson. *Fundamentals of Aerodynamics - 4th Edition*. McGraw-Hill, 2007.

- [33] J.D. Anderson. *Introduction to Flight - 6th Edition*. McGraw-Hill, 2008.
- [34] S.H. Rhee, B.P. Makarov, H. Krishinan, and V. Ivanov. Assessment of the volume of fluid method for free-surface wave flow. *J. Mar. Sci. Technol.*, 10:173–180, 2005.
- [35] T. Begnal. *Popular Woodworking - Pocket Shop Reference*. Popular Woodworking Books, 2006.
- [36] R.A. Moolenaar. *CFD for Sailing Yachts - Validation of the nonlinear free surface potential flow code RAPID (Master Thesis)*. TU Delft, 2010.
- [37] R.A. Moolenaar. Private communication. 2010.
- [38] O.C. Ferrell and M.D. Hartline. *Marketing Strategy*. Thomson South-Western, 2005.
- [39] N. Parolini. Private communication. 2010.

# List of Figures

2.1	The 366 hull as used in the simulations. The top view displays the sections of the hull, together with a side contour. The bottom view displays the waterlines. Geometry from Ref. [9, 10]	10
2.2	The planforms of the different keels. From Ref. [9]	10
2.3	Turbulent flat plate boundary layer. The arrows indicate the two Wall Laws, which apply in the viscous sublayer and in the Log layer. The exact starting position of the outer layer depends on the Reynold's number. The Linear and Log Law are from Ref. [14, 15], the simulation is a near-wall simulation (wall $y^+ = 0.02$ ), and the experimental results by Coles & Hirst are from Ref [21]	13
2.4	Examples of an unstructured (left) and a structured (right) grid around a 2-dimensional sphere	14
2.5	Different geometries invite different grid layouts. On the right of the previous figure is an O-Grid around a 2-dimensional sphere, while this figure displays a C-Grid around a wing section	14
3.1	Different grids used for calculation of the sphere drag coefficient. The bottom of the grid is the axis of rotation. The finer grid is likely to give more accurate results	17
3.2	Sphere drag coefficient at different Reynold's numbers. The insert is a detail of the $Re = 10^3$ to $Re = 10^6$ region, displaying the absence of a distinct 'drag crisis' in the calculated results. Experimental values from Ref. [29]	18
3.3	The effect of the grid size on the solution error at $Re=1000$ . The gray faced label indicates the grid used in the above calculations	19
3.4	Detail of the NACA 63-010 grid	19
3.5	NACA 63-010 drag coefficient. The Anderson fully turbulent flat plate skin friction line is from Ref. [32]	20
3.6	NACA 63-010F grid, detail of the flattened trailing edge. For a better grid the trailing cells should have been more aligned with the expected streamlines, indicated by the arrow	20
3.7	NACA 63-010F drag coefficient compared to the NACA 63-010 drag coefficient. The flattened edge appears to give an increased drag. The Anderson fully turbulent flat plate skin friction line is from Ref. [32]	21
3.8	Several pathlines of the flow in the trailing edge region, for $Re = 3 \times 10^5$	21
3.9	Time evolution of the free-surface for the broken dam problem. The arrow indicates the position of the waterfront as referred to in the following figure	21
3.10	Progress of the waterfront in time, where $z$ is the horizontal position of the waterfront, and $a = 1.5$ m is it's original horizontal position. Experimental values from Ref. [22]	22
3.11	The experimental setup of the surface piercing foil. From Ref. [34] (flipped horizontal)	22
3.12	The grid around the profile, seen from the top and seen from the side. The fluid flows in from the left	23
3.13	The wave height along the profile. Experimental values from Ref. [34]	23
4.1	Convergence of the hull drag for an increasing number of grid cells. A linear dependency in the Log-Log plot indicates that the grid is in the asymptotic range. The black face label is clearly out of the asymptotic range, in this case the grid is too coarse	26
4.2	Convergence of the keel drag for an increasing number of grid cells. A linear dependency in the Log-Log plot indicates that the grid is in the asymptotic range. The black face labels are clearly out of the asymptotic range, in these cases the grid is too coarse	26
4.3	Additional effect of turbulence stimulation strips on the turbulence intensity of the hull (top) and keel (bottom)	27
4.4	Effect of the rudder on the keel drag and vice versa. The dotted lines indicate the reduced dynamic pressure $q$ . The arrow indicates the actual distance	28
4.5	The relative drag increase versus the surface roughness diameter. Clearly a roughness up to 0.02 mm does not effect the drag	29
5.1	The finest grid used for the calculation of the bare hull drag coefficient	31
5.2	An example of the time convergence of the drag coefficient. The fit is a periodic function with an exponentially decaying amplitude	32
5.3	Richardson Extrapolation of the bare hull drag coefficient. The grids have an average cell length ranging from 1.1 % to 2.6 % of the ship's length. The left label indicates the extrapolated value	33
6.1	The medium grid used for the calculation of the Keel 1 drag coefficient. The detail on the right illustrates the C-grid around the keel and the high cell density at the trailing edge	35
6.2	Example of the time convergence of the hull drag for the Keel 3 case	36

6.3	Richardson Extrapolation of the Keel 1 drag coefficient. The different grids have an average cell length ranging from 3% to 7% of the keel's chord. The grey faced label indicates the extrapolated value with error bars . . . . .	37
6.4	Comparison of the free-surface height along the hull, taken from the present Keel 1 simulation and from a potential flow simulation. The present data is for a VOF fraction from 0.4 to 0.6. The potential flow results by Moolenaar are from Ref. [36, 37] . . . . .	38
7.1	The velocity reduction and turbulence experienced by the rudder, as a function of the rudder distance behind the trailing edge of the keel. The arrow indicates the actual rudder distance . . . . .	42
7.2	The velocity reduction (top) and turbulence (bottom) experienced by the rudder for different Froude numbers. The Reynold's number has been scaled accordingly . . . . .	43
7.3	The Reynold's number dependency of the velocity reduction at two different positions behind the keel trailing edge. The resulting slopes are displayed in the following figure. Typically $Re_{model} = 4 \times 10^5$ and $Re_{full\_scale} = 7 \times 10^6$ . . . . .	44
7.4	The effect of a different Reynold's number on the velocity reduction (top) and the turbulent intensity (bottom). The slopes are determined as in the previous figure. The arrow indicates the actual distance . . . . .	45
7.5	The total drag versus the skin friction. Application of the form factor method relies on a linear dependency of these variables . . . . .	47
7.6	The skin friction compared to the ITTC-57 ship correlation line [13] and the Anderson turbulent flat plate friction line [32]. Typically $Re_{model} = 4 \times 10^5$ and $Re_{full\_scale} = 7 \times 10^6$ . . . . .	48
7.7	The observed skin friction divided by: the ITTC-57 Ship Correlation Line [13] (left), and divided by the Anderson turbulent flat plate friction line [32] (right). The form factor method relies on a constant value of these ratios for each keel. Typically $Re_{model} = 4 \times 10^5$ and $Re_{full\_scale} = 7 \times 10^6$ . . . . .	49

# List of Tables

2.1	Hull Dimensions [8] . . . . .	10
2.2	Appendage Dimensions [9] . . . . .	11
6.1	First cell width and wall $y+$ . . . . .	36
6.2	Drag Coefficients: The values observed in the simulation compared to the experimental values. The last column indicates the validity of the simulation, where $A$ indicates that the difference between simulation and experiment is within half the error, $B$ indicates that the difference is within the error, and $C$ indicates that the difference is larger then the error . . . . .	37
B.1	Different Froude Number - wall $y+$ . . . . .	60
B.2	Re Scaling Keel 1 - wall $y+$ . . . . .	60
B.3	Re Scaling Keel 3 - wall $y+$ . . . . .	60



# Appendix A

## Symbols and Acronyms

Symbol	Description	Page	Literature
$\epsilon$	turbulent dissipation rate	12	[14, 15, 18]
$\mu$	dynamic viscosity	9	[11, 14, 15]
$\nu$	kinematic viscosity, not used in this report	-	[11]
$\rho$	density	9	[11, 14, 15]
$\tau$	shear stress	12	[14, 15]
$\hat{\tau}$	stress tensor	11	[11, 14, 15]
$\Omega$	computational domain	11	[15]
$c$	chord	10	[8, 9, 32]
$C_D$	drag coefficient	9	[11, 12]
$C_F$	skin friction drag coefficient	46	[11, 12]
$C_T$	(total) drag coefficient	46	[11, 12]
$F$	drag force	9	[11]
$Fn$	Froude number	9	[8, 9, 12]
$g$	gravitational acceleration	9	
$h$	simulation result for any variable	14	[25]
$I$	unit tensor	11	[11, 14, 15]
$k$	turbulent kinetic energy	12	[14, 15, 18]
$L$	typical model size	9	[11]
$p$	convergence order	15	[25, 26]
$\bar{p}$	pressure	11	[11, 14, 15]
$q$	dynamic pressure $\frac{1}{2}\rho u^2$	28	[11]
$r$	grid refinement rate	15	[25, 26]
$Re$	Reynold's number	9	[8, 9, 11, 12]
$S$	wetted surface	10	[8, 9, 12]
$u$	velocity	11	[11, 14, 15]
$u_\infty$	far-field or inflow velocity	9	[11]
$u^+$	dimensionless flow velocity	12	[14, 15]
$x$	coordinate in flow direction	11	
$y$	coordinate in starboard direction	11	
$y^+$	dimensionless wall distance	12	[14, 15]
$z$	coordinate in upward direction	11	

Acronym	Description	Page	Literature
CAMI	Coated Abrasives Manufacturers Institute	29	[35]
CFD	Computational Fluid Dynamics	7	[2, 12, 14, 15]
CPU	Central Processing Unit (processor)	17	
DSKS	Delft Systematic Keel Series	19	[8]
GB	Gigabyte	12	
GCI	Grid Convergence Index	14	[25, 26]
IACC	International America's Cup Class	10	[8]
ITTC	International Towing Tank Committee	10	[8, 9, 12, 13]
LWL	Length over Water Line	10	[8, 9, 12]
NACA	National Advisory Committee for Aeronautics	19	[11]
RAM	Ready Access Memory	12	
RANS	Reynold's Averaged Navier-Stokes (Equations)	11	[14, 15]
SWOT	Strengths, Weaknesses, Opportunities, and Threats	50	[38]
VOF	Volume of Fluid (Method)	12	[14, 22]

# Appendix B

## Details for Chapter 7

These calculations are run on the same grids as in the keel validation cases. However, since they are at different Reynold's numbers I report the new wall  $y_+$  values. It can be seen that the keel side values are within range. The hull values are mostly out of range, such that the simulations will not give reliable results for the hull drag.

Table B.1: *Different Froude Number - wall  $y_+$*

$Fn$	$\mu$ <i>Pa s</i>	$g$ <i>m s<sup>-2</sup></i>	Bare Hull wall $y_+$	K1 Hull wall $y_+$	K1 Keel
0.325	0.001142	11.38	$39 \pm 16$	$70 \pm 23$	$1.15 \pm 0.45$
0.3	0.001230	13.35	$37 \pm 15$	$65 \pm 22$	$1.08 \pm 0.42$

Table B.2: *Re Scaling Keel 1 - wall  $y_+$*

$\mu$ <i>Pa s</i>	$Re$ $\times 1000$	Coarse Grid wall $y_+$	Medium Grid wall $y_+$
0.001054	394	1.76	1.28
0.001491	279	1.32	0.92
0.002108	197	0.99	0.68
0.002981	139	0.74	0.50
0.004216	098	0.54	0.37
0.005962	070	0.39	0.27

Table B.3: *Re Scaling Keel 3 - wall  $y_+$*

$\mu$ <i>Pa s</i>	$Re$ $\times 1000$	Coarse Grid wall $y_+$	Medium Grid wall $y_+$
0.001054	600	4.05	3.97
0.001491	424	2.96	2.99
0.002108	300	2.16	2.17
0.002981	212	1.58	1.58
0.004216	150	1.16	1.16
0.005962	106	0.85	0.86

# Appendix C

## FLUENT Settings

This appendix contains detailed information on the settings used in the different simulations. I used FLUENT 6.3.26. The listed settings are only those different from default.

### C.1 Benchmark Problems

#### Sphere Drag

Define → Models → Energy  
x Energy Equation  
Define → Models → Viscous  
x k-epsilon  
x Realizable  
x Enhanced Wall Treatment  
Define → Models → Solver  
x Axisymmetric  
Define → Boundary Conditions  
Inflow  
v = 1 m/s  
Turbulence Intensity = 0.001 %  
Turbulence Length Scale = 0.001 m  
Side  
x moving wall; v = 1 m/s  
Define → Materials  
Density = 1  
Viscosity = change this variable for different Re  
Solve → Controls → Solution: 2nd upwind  
Solve → Monitors → Residual  
Convergence Criteria: Standard (0.001 for all residuals)  
*Iterate*

#### NACA 63-010 and 63-010F Section

Define → Models → Energy  
x Energy Equation  
Define → Models → Viscous  
x k-epsilon  
x Realizable  
x Enhanced Wall Treatment  
Define → Materials  
Add water-liquid  
Define → Boundary Conditions  
Inflow  
v = change this variable for different Re m/s  
Turbulence Intensity = 0.001 %  
Turbulence Length Scale = 0.001 m  
Side  
x moving wall; v = 1 m/s  
Fluid  
Water - liquid  
Solve → Controls → Solution: 2nd upwind  
Solve → Monitors → Residual  
Convergence Criteria: Standard (0.001 for all residuals)  
*Iterate*

#### Broken Dam

Define → Models → Multiphase  
x VOF  
x Explicit  
x Impl. Body Force  
o Open Channel Flow  
Define → Models → Solver  
x Implicit  
x Unsteady  
Define → Models → Energy  
o Energy Equation  
Define → Models → Viscous  
x k-epsilon  
x Realizable  
x Enhanced Wall Treatment  
Define → Materials  
Add water-liquid  
Define → Phases  
Air phase 1  
Water phase 2  
Define → Operating Conditions  
Pressure (x, y) = (3, 3)  
x Gravity (x, y) = (0, -9.81)  
Solve → Controls → Solution: 2nd upwind  
Solve → Monitors → Residual  
Convergence Criteria: Standard (0.001 for all residuals)  
*Iterate: 0.02 s*

#### Surface Piercing Hydrofoil

Define → Models → Multiphase  
x VOF  
x Explicit  
x Impl. Body Force  
o Open Channel Flow  
Define → Models → Solver  
x Implicit  
x Unsteady  
Define → Models → Energy  
o Energy Equation  
Define → Models → Viscous  
x Laminar  
Define → Materials  
Add water-liquid  
Define → Phases  
Air phase 1  
Water phase 2

```

Define → Operating Conditions
  Pressure (x, y, z) = (-2, 0, 0.2)
  x Gravity (x, y, z) = (0, 0, -9.81)
Define → Boundary Conditions
  - Water Inflow
    - mixture
      - v = 1.27 m/s
    - water
      - multiphase VOF=1
  - Air Inflow
    - mixture
      - v = 1.27 m/s
    - water
      - multiphase VOF=0
  - Water Outflow
    - Flow Rate Weighting = 0.3
  - Air Outflow
    - Flow Rate Weighting = 0.025
Note: it would have been better to use pressure outlets
Solve → Controls → Solution
  - Pressure = PRESTO!
  - Momentum = 1st Upwind
  - Volume Fraction = Geo-Reconstruct
Solve → Initialize → Initialize
  From Water Inflow
Solve → Initialize → Patch
  Water VOF = 0 for Air
Solve → Monitors → Residual
Convergence Criteria: Standard (0.001 for all residuals)
Iterate: 0.02 s, 50 steps
Define → Models → Viscous

```

```

x k-epsilon
x Realizable
x Standard Wall Function
Define → Boundary Conditions
  Water Inflow
    Turbulence Intensity = 0.001 %
    Turbulence Length Scale = 0.001 m
  Air Inflow
    Turbulence Intensity = 0.001 %
    Turbulence Length Scale = 0.001 m
Solve → Initialize → Patch
  Turbulent Kinetic Energy = 2.4E-10
Iterate: 0.02 s, 150 steps
Define → Models → Energy
  x Energy Equation
Iterate: 0.02 s, 50 steps
Solve → Controls → Solution
  1st order upwind → 2nd order upwind
Iterate: 0.02 s, 150 steps
File → Interpolate → Write ... filename
File → Read → Case: Fine Mesh
Check all settings, many will have changed
File → Interpolate → Read ... filename
Set to Laminar 1st upwind
Iterate: 0.02 s, 10 steps
Set to k-epsilon 1st upwind
Iterate: 0.02 s, 10 steps
Set to k-epsilon 2nd upwind
Iterate: 0.02 s, 750 steps

```

## C.2 Validation for the Bare Hull

These are the settings for the fine grid (94 cells over LWL). The settings for the other grids are similar.

waterout: udf static-pressure  
tankside: moving wall 1.8 m/s

### Bare Hull

```

Define → Models → Solver: x Unsteady
Define → Models → Multiphase:
  x vof
  x explicit
  x implicit body force
Define → Models → Viscous:
  x k-epsilon
  x Realizable
  x Standard Wall Function
Define → Materials: add water-liq
Define → Phases: 1 air / 2 water
Define → Op. Conditions:
  op. press. = 0
  x,y,z = -3,0.5,0.1
  gravity = 0,0,-9.81
  x spec. op. dens.
Define → Boundary Conditions:
  airin
    v = 1.8 m/s
    Turb. Int. = 0.001%
    Turb. Length Sc. = 0.001 m
  waterin
    v = 1.8 m/s
    Turb. Int. = 0.001%
    Turb. Length Sc. = 0.001 m
    vof = 1 (under water)

```

Iteration sequence was: 1st upwind, default urf's, 0.01 s 50 steps. Then 2nd upwind, half urf's, continue 0.01 s steps.

This is the udf file. Actually, for the bare hull I used water density of  $998.2 \text{ kg m}^{-3}$ , for the keel hull combination I used  $999 \text{ kg m}^{-3}$ .

```

#include "udf.h"
DEFINE_PROFILE(static_pressure, thread, position)
{
  real x[ND_ND];
  real zcoor;
  face_t f;

  begin_f_loop(f, thread)
  {
    F_CENTROID(x, f, thread);
    zcoor = x[2];
    F_PROFILE(f, thread, position) =
      -9.81*999*zcoor;
  }
end_f_loop(f, thread)
}

```

## C.3 Validation for the Keel Hull Combination

These are the settings for the coarse grid (16 cells over keel chord). The settings for the other grids are similar.

```
Keel 1
Define → Models → Solver: x Unsteady
Define → Models → Multiphase:
  x vof
  x explicit
  x implicit body force
Define → Models → Viscous:
  x k-epsilon
  x Realizable
  x Enhanced Wall Treatment
Define → Materials:
  add water-liq
  water density = 999 kg m-3
  water viscosity = 0.001054 kg/m/s
Define → Phases: 1 air / 2 water
Define → Op. Conditions:
  op. press. = 0
  x,y,z = -3,0.5,0.1
  gravity = 0,0,-9.81
  x spec. op. dens.
Define → Boundary Conditions:
  airin
    v = 1.8 m/s
```

```
Turb. Int. = 0.001%
Turb. Length Sc. = 0.001 m
waterin
  v = 1.8 m/s
  Turb. Int. = 0.001%
  Turb. Length Sc. = 0.001 m
  vof = 1 (under water)
waterout: udf static-pressure
tankside: moving wall 1.8 m/s
Solve → Controls → Solution: all urf's 0.1
Solve → Initialize → Initialize: from waterin
Adapt → Region → Mark: z positive
Solve → Initialize → Patch: water vof = 0 to marked register
```

The iteration sequence was: Set air viscosity to 0.0017894 kg/m/s, 1st upwind, iterate 0.02 s 50 steps. Reset air viscosity to default 1.7894e-5 kg/m/s, iterate 0.02 s 25 steps. Change to 2nd upwind, iterate 0.02 s for number of steps.

The Keel 3 iteration sequence was different. After resetting the air viscosity I iterated 1st upwind until the hull drag had converged, at flowtime roughly 8 seconds. Only then I changed to 2nd upwind.

# Appendix D

## What did not work ...

This appendix contains some information on what did not work, when setting up the simulations.

### D.1 Benchmark Problems

Somehow, when going from a laminar to  $k-\epsilon$  viscous model during computation of the problem, the turbulent kinetic energy can diverge within several iterations. This does not happen when, after changing to  $k-\epsilon$  and before continuing iterations, a small turbulent kinetic energy (corresponding to the inflow settings for turbulence intensity and dissipation rate) is patched to the complete domain.

Going directly from coarse 2nd upwind  $k-\epsilon$  to fine 2nd upwind  $k-\epsilon$  (refinement in FLUENT), the solution would diverge. With some 10 iterations with laminar and then 1st upwind  $k-\epsilon$  the solution would behave as expected.

The FLUENT User's Guide recommends 'open channel flow' for problems like the surface piercing hydrofoil. However I had difficulties with setting the correct boundary conditions (presumably for the mass flow inlet) and could thus not run the problem under 'open channel flow' settings.

### D.2 Validation for the Bare Hull

Since the simulation is unsteady and results in an oscillating drag coefficient, calculations times a very long. They can be reduced by decreasing the grid size, which is only tolerable if one applies a proper grid convergence study and/or Richardson Extrapolation.

Interpolating coarse grid results for initialization of finer grids did not work. This is mainly due to distortion of the free-surface. This might have been solved by interpolation followed by patching of a level free-surface; or by first simulating laminar a couple of steps. However I did not realize this at this point, and initialized every simulation from scratch.

Because I'm interested in the final steady solution, it would be possible to run an implicit vof scheme. However, this does not provide Geometric Reconstruction and therefore leads to a smudged free-surface.

### D.3 Validation for the Keel Hull Combination

It should be stressed that the keel hull combination is much more complicated than the bare hull. I started out with simulating the bare hull, which took 3 weeks. With this experience, and also part of the geometry ready to go, it took me almost 3 months to complete the keel hull combination simulations.

This kind of simulation is likely to run into several difficulties. The main challenges are to limit the amount of grid cell size increase or decrease, even more so than in the cases stated above. The problem of having a structured grid for a foil, is that a structured grid fill not represent an infinitely thin trailing edge. Fortunately, such a trailing edge would lead to vibrations in practical use. This is the reason that the foils studied here all have flattened trailing edges, with a width in the order of 1 - 2 mm. This effectively means that the grid cell size near the trailing edge would be in the order of 0.2 mm. This being said, the grid effectively contains areas with a large increase or decrease of grid cell size. If this increase or decrease is to large, this will result in very high turbulence and in distortion of the free-surface. Also, a repeating challenge is the proper initialization. I have tried an array of different 'smart' initial conditions, and expected to be able to use the coarse solution as initial condition for the finer grid. However, how much I tried, this would not work in any way. Even interpolation with successive patching of low turbulence combined with a level free surface would diverge within several time steps. Also, ramping the inflow speed from 0.0 m/s to 1.8 m/s over a flow time of 1.0 s did not result in a stable simulation.

Another problem is the difference in Reynold's number of the air and the water. Where the water behaves quite nicely, the air is at a much higher Reynold's number and is likely to cause unexpected high amounts of turbulence. This can be frustrating, since in this stage the behavior of the air is likely to be of minor importance in the actual problem.

My approach was to initially increase the air viscosity by a factor of 100 or 1000, and restore it to its actual value after typically 1 s of flow time.

Contrary to common sense, it is not very easy to create a finer grid from a coarser one. In my experience, the coarse grid might converge nicely. A simply refined grid might then however not converge at all. Especially the grid cells near the keel's trailing edge need a lot of attention. This is quite different from the bare hull case, where grid refinement was completely straightforward. Needless to say, all three grids should have proper wall cell sizes to reach a tolerated wall  $y^+$ .

All in all the most important problems do not appear to arise from the solver but from the grid itself. Creating a well behaving 38 block-structured-grid capable of 3d free-surface simulation is, in my opinion, close to the limits of the practical possibilities of the grid generator GAMBIT.

## D.4 General Suggestions

- When GAMBIT freezes it is often possible to press the close window 'X' button, then select 'cancel' at prompt. This will usually revive GAMBIT.
- Sometimes GAMBIT mesh faces are distorted. To solve this, localize the problem edge and make a new NURBS edge close to it, with the same endpoints. Then, for example, split the surface and glue the little part to another surface.
- When GAMBIT reports "identifier open" delete the associated .lok file
- To save all currently-defined boundary conditions to a file, select the write-bc text command and specify a name for the file. Use file > write-bc and file > read-bc
- For high resolution images from FLUENT: Make a file → hardcopy: EPS vector 500 dpi file, and specify line width under display → options